An Extended Scalar Sector: Charged Higgs and Dark Matter

Mahdi Poormohammadi

Dissertation for the degree of Philosophy Doctor (PhD)

Department of Physics and Technology
University of Bergen

June 2013

Acknowledgements

In carrying out my study I am indebted to many people, including my teachers, colleagues and friends. The first and the most, I would like to thank my supervisor professor Per Osland, who provided me with the concept for this thesis, for his academical and partially financial support throughout my study. Without his help and instructions, I would not be able to complete this thesis.

Acknowledgments are also given to the Norwegian Research Council for partial financial support.

I also would like to extend my gratefulness to my co-supervisors, professor Anna Lipniacka at the University of Bergen and Dr. Odd Magne Ogreid at Bergen College.

I have been aided by several individuals. Dr. Marco Pruna has generously provided support both in developing and implementing our model in CalcHEP and giving me the opportunity to interact and work with him. My words can certainly not express how much he has been beneficial to me in my studies. Dr. Florian Bonnet has been the source of invaluable information about the code MadEvent. Even though I have never met him in my life, he has been replying to my emails promptly and patiently. I would like to thank Dr. Nils-Erik Bomark with whom I shared my office and who was always available to answer my questions.

I am extremely grateful about the atmosphere prevalent in the Department of Physics and Technology. I scientifically benefited from all people on the third floor.

Some moments are so dumb that one could not even share them with one's parents, but God has created friendship and friends for these moments. In this regard, I thank Sirus Seraji and his kind family. My thankfulness likewise extends to all my friends for their encouragements and understanding in my odd hours.

My special thanks go to Barbara for her being very patient during the last 3 years and her trying to be supportive. Furthermore, I am deeply indebted to my family and parents. Their love is always supportive, encouraging and invaluable with no expectation! They never became displeased even though I could only meet them once in a long while!

I thank the Journal of High Energy Physics for allowing me to use the papers in the thesis.

Mahdi Purmohammadi

Abstract

Despite the great success of the Standard Model in describing many aspects of the experiments, there are compelling reasons that it needs to be improved. One of the major mysteries physics has been exploring is the composition of matter in the Universe. The density of the luminous matter $\Omega_{\rm lum}$ is thought to be about 4% of the total energy density $\Omega_{\rm tot}$ of the Universe. Dark Matter makes up $\sim 26\%$ of the energy density of the Universe which is inferred by its gravitational effects and bending of light from luminous matter as well as the geometry of the Universe. Over the last few years the paradigm of DM has shifted towards the subatomic Weakly Interacting Massive Particles (WIMPs). Thus, the existence of DM is one of the most important pieces of evidence for physics Beyond the Standard Model (BSM). The observation of DM will presumably indicate that there is a new particle.

The discovery of the Higgs particle paves the way beyond the SM for exploring the existence of new particles and the component of dark matter. There are several attempts to extend the SM and include the new physics. The Two-Higgs-Doublet Model (2HDM) is one of those. This model offers a new spectrum of scalar particles. These particles can accommodate additional CP violation in the neutral sector of the Higgs potential. These particles can be produced at accelerators. If they are produced, they will decay to SM particles via a chain of decay modes. Their signals can be discerned against the SM background, by means of a set of feasible techniques. From this point of view, one good avenue in search for physics beyond the SM is to search for new charged particles. In the context of the 2HDM, the charged Higgs bosons can be produced in association with quarks, neutral Higgs bosons and the W bosons. The production rate of the charged Higgs bosons along with the neutral Higgs bosons is too low to give rise to visible signals over the SM background. But the other channels hold promises. In particular, the event analysis of the charged Higgs boson produced in association with the W boson leads to a number of surviving signal events after passing a set of filters.

There are also extensions to the SM that accommodate a DM candidate. Let us consider the 2HDM extension of the SM model. The 2HDM could be equipped with an extra doublet which is inert in the sense that it has zero vacuum expectation value and does not couple to fermions. Therefore the resulting model is refereed to as CP-violating Inert Doublet Model (or IDM2). The lightest neutral member of the model, by help of an ad hoc Z_2 symmetry, is stabilized to contribute to the missing mass of the Universe.

The IDM2 is viable in two different mass domains of the DM candidate, namely low and high mass regions. The model can naturally reproduce the observed DM abundance due to effective DM self-annihilation in the early Universe in the low-mass region which is within reach of the LHC experiments at CERN. These experiments might illuminate our understanding of the nature of the DM. Besides, parameter points in the

low mass region pass the constraints from the latest experiments in search for DM both in direct and indirect ones. Due to the nature of the imposed symmetry, the members of the inert doublet will be produced in pairs. In a suitable part of the parameter space the masses of the particles could be very close and therefore the decay is inhibited by phase space, and they can fly away from the interaction point before they decay to SM particles or escape the detector. In this case, the charged members of the inert doublet will lead to so-called displaced vertices and decay to charged leptons or jets and the DM candidate somewhat away from the interaction point.

In case of the single production of the charged scalar, the experimental signature would be the observation of a track from the interaction point up to the decay vertex. In the decay vertex there will be a kink corresponding to the decay and a track of the charged lepton, if the charged scalar decays leptonically, or two jets, if the charged scalar decays hadronically. The kinematic properties of the jets depend on the mass of the charged scalar and the mass splitting of the charged and dark matter particles. If the mass splitting is below a couple of GeV, the displaced vertex could be realized. For mass splitting above a few GeV, one might be able to identify the hadronic decay of the charged scalar. A production channel for the charged scalar can also contain an extra hard jet. This extra jet can help in triggering the charged scalar. Therefor, the decay of the charged scalar may give unique signals that might enable physicists to detect them.

List of papers

1. L. Basso, A. Lipniacka, F. Mahmoudi, S. Moretti, P. Osland, G. M. Pruna, M. Purmohammadi, *Probing the charged Higgs boson at the LHC in the CP-violating type-II 2HDM*, JHEP **1211**, 011 (2012).

2. B. Grzadkowski, O. M. Ogreid, P. Osland, A. Pukhov, M. Purmohammadi, *Exploring the CP-Violating Inert-Doublet Model*, JHEP **1106**, 003 (2011).

3. P. Osland, A. Pukhov, G. M. Pruna, M. Purmohammadi, *Phenomenology of charged scalars in the CP-Violating Inert-Doublet Model*, JHEP **1304**, 040 (2013).

Contents

Acknowledgements **i**

Abstract **iii**

List of papers **v**

1 Introduction **1**

2 The Standard Model **3**
2.1 Introduction to Gauge Symmetries of Weak Interaction 4
2.2 Symmetry Properties 4
2.3 Chiral Fermion State 8
2.4 Spontaneous Symmetry Breaking 9
2.5 The Higgs Mechanism 10
2.6 The Electroweak Theory of Weinberg and Salam 14

3 Challenges for the Standard Model **17**
3.1 Introduction 17
3.2 Baryon Asymmetry 17
3.3 Naturalness and Gauge Hierarchy Problem 19
3.4 The Dark Matter Problem 21
3.4.1 Dark Matter and Evidence for its Existence 22
3.4.2 WIMP Dark Matter and Favoured Candidates 23

4 Charged Higgs Production in type II 2HDM **25**
4.1 Introduction 25
4.1.1 The Fields 25
4.1.2 The Potential and Parameters 26
4.1.3 BRs of Charged and Lightest Neutral Higgs Bosons 27
4.2 Charged Higgs Bosons at the LHC 29
4.2.1 Cross Section Analysis for the Benchmark Points 30
4.2.2 Simulation of Signal and Background Events 32

5 Two Higgs Doublets plus an Inert Doublet, the IDM2 **43**
5.1 Introduction 43
5.2 Features of the Model 43
5.2.1 The Fields 44
5.2.2 The Potential 44

5.2.3 Dark Democracy 45
5.3 The Parameters of the Model 45
5.4 Allowed Parameter Domains 46
5.4.1 Medium Dark-Matter Mass Regime 46
5.4.2 High Dark-Matter Mass Regime 47

6 Phenomenology and LHC Prospects of the IDM2 **51**
6.1 DM Identification 51
6.1.1 Direct Detection 51
6.1.2 Indirect Detection 52
6.2 Collider Signals 53
6.2.1 Charged Scalar Production at the LHC 54
6.2.2 Associated production of $\eta^+ S$ and $\eta^- S$ 55
6.2.3 Associated production of $\eta^+ SX$ and $\eta^- SX$: 55
6.2.4 Pair Production of Two Charged Particles, $\eta^+\eta^-$ 55
6.2.5 Decay of Charged scalars 57
6.2.6 Displacement of the Decay Vertex 57

7 Summary and conclusions **61**

Scientific results **67**
7.1 Probing the charged Higgs boson at the LHC in the CP-violating type-II 2HDM 69
7.2 Exploring the CP-Violating Inert-Doublet Model 115
7.3 Phenomenology of charged scalars in the CP-Violating Inert-Doublet Model 157

List of Figures

2.1 Coupling of four fields (left panel) and coupling of two independent fields (right panel). 13

3.1 One loop radiative corrections to the Higgs squared mass parameter from a) quartic Higgs self-coupling, b) gauge boson loops, c) heavy fermion loops f. 20

4.1 Branching ratios of the charged Higgs versus mass for six benchmark with $\tan\beta = 1$. Similar results were given in [34]. 28
4.2 Branching ratios of the charged Higgs versus mass for two benchmark points. Here, $\tan\beta = 2$. Similar results were given in [34]. 29
4.3 Partonic contributions to single charged Higgs production). 30
4.4 Production cross sections vs the charged Higgs mass for $\sqrt{s} = 8$ (dashed line) and $\sqrt{s} = 14$ (solid line) for benchmark points $1-4$. Similar results are presented in [34]. 31
4.5 Similar to figure 4.4, for benchmark points $5-8$. Similar results are presented in [34]. 32
4.6 $M(b\bar{b}jj)$ vs. $M_T(b\bar{b}\ell\nu)$ after cut 5 for (unweighed) point P_5, with $M_{H^\pm} = 310$ GeV (red) and $M_{H^\pm} = 390$ GeV (green). In blue is the (unweighed) top background. Similar figure is presented in [34]. 37
4.7 Points P_1 (left panel) and P_8 (right panel). Number of events integrated with $\mathcal{L}_{\rm int} = 100$ fb^{-1} at $\sqrt{s} = 14$ TeV vs $M(b\bar{b}jj)$ for signal (colored lines) and t-quark background. 40
4.8 Point P_2. Similar to figure 4.7. 40
4.9 Point P_3. Similar to figure 4.7. 40
4.10 Point P_4. Similar to figure 4.7. 41
4.11 Point P_5. Similar to figure 4.7. 41
4.12 Point P_7. Similar to figure 4.7. 41

5.1 Allowed regions in the $M_{\eta^\pm} - m_\eta$ plane, for DM mass $M_S = 60$ GeV and $M_S = 75$ GeV, with lightest Higgs mass $M_1 = 120$ GeV [39]. 47
5.2 Allowed regions in the $M_{\eta^\pm} - m_\eta$ plane, for $M_S = 550$ GeV, $M_A = 551$ GeV (left panel), and $M_S = 800$ GeV, $M_A = 801$ GeV (right panel) with $M_1 = 120$ GeV. The thin solid line indicates $m_\eta = M_S$, whereas the dashed line gives $M_{\eta^\pm} = M_A$ [39]. 48
5.3 $M_S = 3000$ GeV and 5000 GeV, both with $M_1 = 120$ GeV [39]. 49

6.1 Direct-detection WIMP-nucleon cross sections compared with the CDMS-II (dashed) and XENON100 (solid) bounds. 52
6.2 Fermi-LAT bounds on the velocity weighted annihilation cross section for $SS \to \gamma\gamma$. 53
6.3 Direct production channels. 54
6.4 Cross sections for $\eta^+ S$ and $\eta^- S$ associated production at $\sqrt{s} = 14$ TeV. Left: Individual cross sections for $\eta^+ S$ and $\eta^- S$. Right: Sum. Similar results are shown in [55]. 55
6.5 Cross sections for $\eta^+ S$j and $\eta^- S$j associated production at $\sqrt{s} =$ 14 TeV. Left: Individual cross sections for $\eta^+ S$j and $\eta^- S$j. Right: Sum. Similar results are shown in [55]. 56
6.6 Cross sections for $\eta^+ \eta^-$ pair production at $\sqrt{s} = 14$ TeV. Left: P_3, Right: P_5. Similar results are shown in [55]. 56
6.7 Decay of a charged scalar η^+ to the DM particle S, a charged lepton and a neutrino. 57
6.8 Left: Decay width of the $\eta^\pm$. Right: $\eta^\pm$ branching ratios to S or A, plus two fermions [55]. 58
6.9 Decay length λ vs. mass splitting $M_{\eta^\pm}$–M_S for two relative S–A spectra [55]. 58

List of Tables

2.1 Symmetries and the associated conservation laws. 5

4.1 Benchmark points selected from the allowed parameter space [34]. The mass parameter μ, the mass M_2 and allowed range of $M_{H^\pm}$ are in GeV. 27
4.2 BRs of the lightest neutral Higgs, BR$(H_1 \to XY)$, for the benchmark points. Similar results are presented in [34]. 30
4.3 Generation cuts. 33
4.4 Consecutive efficiency of the cuts imposed on the top quark background and on the benchmark points P_2, P_4 and P_5 with $M_{H^\pm} =$ 310 GeV and $M_{H^\pm} = 390$ GeV. The results are consistent with [34]. 36
4.5 Comparison between C_{squ} and C_{sng} vs M_{lim} for P_2: surviving events and significance with respect to the background. Similar results are also presented in [34]. 37
4.6 Comparison between C_{squ} and C_{sng} vs M_{lim} for P_4: surviving events and significance with respect to the background. Similar results are also presented in [34]. 38
4.7 Comparison between C_{squ} and C_{sng} vs M_{lim} for P_5: surviving events and significance with respect to the background. Similar results are also presented in [34]. 38
4.8 Surviving events and their significance after the single cut of Eq. (4.28) and after the peak selection of Eq. (4.29), for all points of table 4.1, except P_9 and P_{10}. Similar results are also presented in [34]. 39

6.1 Benchmark points selected from the allowed 2HDM parameter space. Some of these points are taken from [55]. Masses are in GeV, $\mu =$ 200 GeV. Values of the ratio $R_{\gamma\gamma}$ are given for the 2HDM, as well as for IDM2. Two values of $M_{\eta^\pm}$ are considered, 100 GeV and 200 GeV. . 54

Chapter 1

Introduction

The most fundamental building blocks of matter are elementary particles. In the course of last century along with the developments in the fields of atomic, nuclear, cosmology and high energy physics, the entity of these particles has changed. Our era's elementary particles are quarks and leptons that along with gauge bosons, mediators of interactions between particles, are well-suited to a beautiful scheme, called the Standard Model (SM), with well-defined calculational rules, agreeing with experiments. The SM of particle physics, suitably extended to include an appropriate neutrino phenomenology, has been the pillar of fundamental physics. A cornerstone of the SM is the mechanism of spontaneous symmetry breaking that, as is well known, is mediated by the Higgs boson. Then, the discovery of the Higgs boson was the highest priority of the Large Hadron Collider (LHC) [1, 2].

The SM requires the existence of a scalar Higgs boson to break electroweak symmetry and provide mass terms to gauge bosons and fermion fields.

The Nobel Prize was awarded for unifying the parts of the theory comprising the weak and electromagnetic forces in the electroweak theory. The remaining sector, strong interactions, is also based on a non-Abelian gauge theory. Gravity is the only fundamental force which is not integrated into the SM and it is one of the main compelling reasons we believe that the SM is not an ultimate theory and we need extensions beyond it or a brand new theory which could contain a consistent quantum theory of gravity. The string theory holds some promise.

In the last decades, scientists who work to understand the fundamental forces of nature and the composition of matter in the Universe, have speculated that there are new forces and new types of particles. The study of the rotations of the galaxies and using the Newtonian dynamics as a good approximation, with the knowledge of the approximate masses of the neighbouring galaxies, reveals that the visible matter is insufficient to cause the observed rotational dynamics of the galaxies. It is then speculated that there must be some invisible matter permeating the Universe. Such matter, if it exists, is gravitationally coupled with the normal matter that we experience in everyday life and is dubbed "dark matter". The idea of dark matter has become very popular in both the literal and the figurative sense over the last decades and it turns out that it has some profound implications for the evolution of the Universe. Such a component is not incorporated into the matter content of the SM.

The SM of particle physics also fails to come up with a reasonably sufficient explanation for the conundrum of baryon asymmetry, the fact that there is more matter than

antimatter in the Universe [3].

In this thesis, our aim will be to outline an extension to the SM which addresses the problem of dark matter by introducing a viable candidate for it and simultaneously expand the scalar sector of the SM. The latter feature of the model brings forward new sources for CP-violation in the scalar sector.

The thesis is organized as follows. In chapter 2, we review electroweak interactions and have pieces of explanation on the Higgs mechanism and the Weinberg-Salam theory for constructing the SM. We see how to approach to the point that spontaneously breaking symmetry of local gauge symmetry causes fermions, leptons and quarks, the electroweak field mediator bosons as well as Higgs bosons to acquire mass.

In chapter 3, it will be briefly demonstrated why we are in need of new physics and since the main goal of the thesis is to introduce a dark matter candidate it will be emphasized that the current picture of particle physics does not encompass a viable dark matter candidate that could explain the matter density of the Universe.

In chapter 4, we present the charged Higgs production and decay in the scope of the Two-Higgs-Doublet Model[1]. It will reveal that with an astute study and search one can see a few events at the LHC to probe the existence and domain of the new physics.

Chapter 5 is dedicated to introducing and exploring the CP-Violating Inert-Doublet Model, IDM2[2], which is home for a dark matter candidate. The model will be presented and its viable parameter space, based on the mass of the dark matter candidate, will be explored and discussed.

Since the new charged scalars of the model could leave some signature at the LHC which enables us to track the new physics beyond the SM, in chapter 6, the aim is to attempt to demonstrate the LHC phenomenology of the model under discussion. The viability of the model will also be checked with bounds from the current direct and indirect detection experiments for dark matter.

A conclusion and outlook is given at the end of the thesis.

[1] In the thesis, this model will be referred to as 2HDM.

[2] Throughout the thesis I will refer to this model as IDM2.

Chapter 2

The Standard Model

The current theory of fundamental particles and how they interact are described by the Standard Model of particle physics. The theory includes three fundamental forces in the Universe, namely,

- strong interactions due to the color charge of quarks and gluons (e.g., the binding force of the hadrons).
- electromagnetic interactions due to the electric charge of fermions which introduces the photon as a mediator.
- weak interactions that introduce heavy gauge bosons as the carrier particles.

Gravitation is the fourth fundamental force which can not be explained by the SM and it is described by Einstein's theory of general relativity. The effects of gravity could be neglected under high energy physics situations because of their tiny contribution. It is worth mentioning that gravity has different mathematical structure and no complete quantum field of gravity has been developed yet. In a way unification of various ideas are one of the main discoveries in physics throughout the ages and the attempt for unification of all these types of forces is a major goal for the particle physics community. Quantum electrodynamics created a quantum theory of electromagnetism and the electroweak theory unified this theory with the weak nuclear force of nature. The quantum chromodynamics describes the strong nuclear force. These three forces are contained in the framework of the SM and it is hoped that unification of gravity with the other forces will create a new version of the SM which could explain how gravity works on the quantum level.

Physicists believe that all four forces were once unified at high energy levels, but with the expansion of the Universe and reduction in its energy into a lower state, the symmetry between the forces began to break down and the symmetry breaking created four distinct forces of nature. So the principle of symmetry is crucial to the study of physics and has special implementations. When we take a system and in some way transform it and nothing seems to change about the measurable physical properties, then a symmetry, otherwise a broken symmetry, exists. Translational symmetry is the most familiar symmetry in physics; a change in the location of objects retains the properties of the system.

2.1 Introduction to Gauge Symmetries of Weak Interaction

Group theory is the natural mathematical language of symmetry. In this section, the global symmetry will be illustrated and then it will be shown how local gauge symmetry can be used to generate dynamics, interactions.

The unitary group $U(N)$ consists of $n \times n$ unitary matrices ($UU^\dagger = U^\dagger U = 1$). $U(N)$ is non-Abelian for $n > 1$ and the Abelian subgroup of this, $U(1)$, will be a set of 1×1 unitary matrices with phase transformations $e^{i\delta}$. The special unitary group, $SU(N)$, which is often present in the theories of particle physics, is a group of $n \times n$ matrices with unit determinant $|U| = 1$ [1]. The study of group structure becomes simplified if one could decompose a group as a direct product of smaller groups. For instance, $U(N)$ could be written as $SU(N) \times U(1)$. The $SU(2) \times U(1)$ is a direct product group with elements that are direct products of $SU(2)$ matrices and the $U(1)$ phase factor. The special unitary groups become manifest in particle interactions. In the notation of group theory, the SM interactions are described as

$$SU(3) \times SU(2) \times U(1) \tag{2.1}$$

where $SU(3)$ is the gauge group of strong interactions, the set of all 3×3 unitary matrices with unit determinant, and $SU(2) \times U(1)$ can reflect the gauge group of the electroweak interaction. Understanding symmetries is crucial to understanding the electroweak sector of the SM.

2.2 Symmetry Properties

In theoretical particle physics, one of the most insightful considerations is that the interactions are governed by symmetry principles. The invariance of the physical system under certain symmetries implies a proper set of conservation laws. There is a tight connection between symmetries and conservation laws in the framework of Lagrangian field theory. For instance, from classical mechanics, we remember that the conservation of energy, momentum and angular momentum were deduced from translational invariance in time, space and rotation. In field theory, relationships between symmetries and conservation laws are described by Noether's theorem. According to the theorem, every symmetry of nature is related to a conservation law and conversely every conservation law to an underlying symmetry. Usually symmetries are categorized into two groups, finite (discrete) or continuous symmetries.

Finite space-time transformations

As the name implies, it is a symmetry that describes changes by a certain amount; hence, non-continuous changes in a system[2]. These groups have finite elements and the Noether theorem does not hold for these transformations and they are multiplicative quantum numbers. In quantum mechanics, inversion transformations are of relevance and importance which in practice are discrete subgroups of continuous groups. Here

[1] In a similar manner, $SO(N)$ is the group of $n \times n$ orthogonal matrices with unit determinant and a subgroup of this $SO(3)$ is just the familiar three-dimensional rotational group.

[2] It seems that physics chooses not to obey these symmetries.

Symmetry $\xrightarrow{\text{Noether's theorem}}$	Conserved quantity
Gauge transformation	Charge
Translation in time	Energy
Translation in space	Momentum
Rotation	Angular momentum

Table 2.1: Symmetries and the associated conservation laws.

three of these transformations are outlined which are important in particle physics. They are all given by unitary operators.

- **Parity transformation**, P, inverts every spatial coordinate with respect to the origin, $P(t,\mathbf{r}) = (t,-\mathbf{r})$, i.e., it changes the sign in left-handed and right-handed reference frame. Intrinsically, particles and antiparticles have opposite parity. A system is parity symmetric if the Lagrangian is invariant under a parity transformation. In this case, there exists a set of phase factors η_p so that[3]

$$P\psi(t,\mathbf{r}) = \eta_p \psi(t,-\mathbf{r}). \tag{2.2}$$

  If interactions are parity symmetric then the transition amplitude also will commute with parity

$$[P,H] = 0 \quad \longrightarrow \quad [P,S] = 0 \tag{2.3}$$

  where H represents the Hamiltonian and S illustrates the scattering matrix. It means that the amplitude links only states of the same parity. There is no evidence for violation of parity in electromagnetic or strong interactions, but it is known that parity conservation is broken under weak dynamics.

- **Charge conjugation**, C, interchanges each particle with its antiparticle without changing momentum and spin. Transformation of a field under C will be of the form

$$C\psi(x) = \eta_c \psi^{\dagger}(x). \tag{2.4}$$

  The only allowed eigenvalues of C are $\eta_c = \pm 1$. Note that in the case of charge conjugation the space-time variable x is the same on both sides of the equation and the Hamiltonian density commutes with C like in the case of P. But unlike parity only very few particles are charge conjugate eigenstates. In effect, C is a unitary operator that reverses every internal quantum number and charge, like baryon number, strangeness or color charge. Therefore, a green down quark of charge $-1/3$ will be charge conjugated into an anti-green down anti quark of charge $1/3$. The idea is that as long as all our charges swap sign, all the forces between them should be the same and nature should look pretty much the same as it would without charge conjugation. It turns out that it is not thoroughly true in the present-day Universe.

[3] In all our illustrations we have picked $\psi(t,\mathbf{r}) = \psi(x)$ to be a Dirac filed.

- **Time reversal operator**, T, reverses sign of the time and thus this reverses time derivatives like momentum, angular momentum and spin. In the general case, and in the language of quantum mechanics

$$T\psi(t,\mathbf{r}) = \eta_T \psi(-t,\mathbf{r}). \tag{2.5}$$

In treating (2.5), one has to be careful. It could take different forms in terms of the spin of particles. Here η_T is a phase factor, a constant matrix. Equation (2.5) implies that

$$\begin{aligned} \mathbf{r}' &= T\mathbf{r}T^{-1} = \mathbf{r}, \\ \mathbf{p}' &= T\mathbf{p}T^{-1} = -\mathbf{p}, \\ \mathbf{s}' &= T\mathbf{s}T^{-1} = -\mathbf{s}, \end{aligned} \tag{2.6}$$

where $\mathbf{p}$ and $\mathbf{s}$ are angular momentum and spin respectively, they change sign on time reversal. If we apply this classical transformations to the commutation relation $i = [\mathbf{r},\mathbf{p}]$, then we can show T can not be unitary:

$$\begin{aligned} TiT^{-1} &= T[\mathbf{r},\mathbf{p}]T^{-1} \\ &= \mathbf{r}'\mathbf{p}' - \mathbf{p}'\mathbf{r}' \\ &= -(\mathbf{r}\mathbf{p} - \mathbf{p}\mathbf{r}) \\ &= -[\mathbf{r},\mathbf{p}] = -i. \end{aligned} \tag{2.7}$$

The anti-unitary nature of T implies that this is an operator which flips the sign of i and has no observable eigenvalues which can be used to label states. So we can not easily check its conservation simply by multiplying numbers as we do in the case of P and C.

Time-reversed states in quantum mechanics are usually complicated and improbable owing to the fact that it is extremely difficult to set up necessary initial conditions. Time reversal could be checked via the *principle of detailed balance* that states $A + B \longrightarrow C + D$ and its reverse $C + D \longrightarrow A + B$ with the corresponding initial conditions should have the same rate in both directions. For a variety of processes, it has been checked and no T violation is revealed for the strong or electromagnetic interactions. It is difficult to reconstruct the same procedure for weak interactions. Nonetheless there are compelling reasons that render T not to be a perfect symmetry.

On a small scale this symmetry is preserved as it makes no difference which direction time is flowing, the physics will stay unchanged, but on a large scale time-flow prefers a specific direction; going forwards and backwards matters and the physics is different. It might be argued that the symmetry breaking is the source of entropy. We expect the weak interaction to violate T, and its violation has been established in K and B mesons decay.

Let us have a brief look at the combined symmetries in the context of particle physics.

CP symmetry: Within the standard $SU(2) \times U(1)$ electroweak model, with only one Higgs doublet, CP conservation is not exact. The CP violation is introduced via complex Yukawa couplings between the fermions and the Higgs boson. The Higgs boson acquires a vacuum expectation value through breaking the $SU(2)$ symmetry and then its interaction with quarks, Yukawa interaction, becomes mass mixing for quarks. The CP violation shows up in complex phases in the mixing matrices. By redefining the phase of various quark fields some of these phases could be removed. CP violation is ubiquitous in theories of new physics.

CPT symmetry: Each of P, C and T symmetries acting alone or even in a pair do not leave a physical system invariant. The SM of particle physics predicts that the simultaneous application of all three transformations must be a symmetry. CPT is required to be conserved in any local quantum field theory.

From the CPT theorem one concludes that for any local hermitian Hamiltonian H, which is invariant under a proper Lorentz transformation that involves neither space nor time inversions, there exists a choice of the phases, η_p, η_c and η_T, such that H commutes with the product of the operators P, C and T. CPT is basically the combined action of all three transformations that mandates particles and antiparticles must have certain identical properties, such as the same mass, lifetime, charge and magnetic moment. This is why we believe that if CP is violated in nature there must be a compensation to it to make CPT conserved, so T must also be violated.

Continuous space-time symmetries

In continuous groups the elements depend on one or more continuous parameters. We are interested in internal symmetry transformations such as isospin, color and flavour symmetries. These symmetries do not mix fields with different space-time properties. In other words, these transformations commute with the space-time components of the fields and therefore leave the Lagrangian invariant, but they can transform one particle into another, rendering the same mass, but different quantum numbers. Continuous symmetries have additive quantum numbers. There are two broad categories of discussion:

Global phase transformation: One of the internal degrees of freedom is codified in the form of a phase of the wave function. The Lagrangian of a reasonable theory is invariant under a phase transformation of

$$\psi(x) \longrightarrow U\psi(x)$$
$$U = e^{i\alpha} \tag{2.8}$$

where α is a phase factor and it takes any real value. This phase transformation might be thought of as a multiplication of ψ by a unitary 1×1 matrix, group of $U(1)$, and the symmetry is called $U(1)$ gauge invariance.

Local gauge transformation: The locally-symmetric theories enable us to derive the physics. This class of symmetry transformations can be expressed as

$$\psi(x) \longrightarrow e^{i\alpha(x)}\psi(x). \tag{2.9}$$

Here the differentiable phase, $\alpha(x)$, has space-time dependency, it is a function of x^μ, and in this sense is more general. The derivative of the transformation $\partial_\mu(e^{i\alpha(x)}\psi(x))$ leads to new terms in the Lagrangian and to cancel them we have to introduce new fields and it turned out to be the case for the SM of particle physics.

The idea of local gauge invariance goes back to the work of Hermann Weyl in 1918 [4]. The idea of locally symmetric transformations later in 1954 by Yang and Mills was applied to the group $SU(2)$ and extended to $SU(3)$ color symmetry [5].

2.3 Chiral Fermion State

The projection of the spin of the particle onto the direction of its momentum is called helicity

$$\text{Helicity} \equiv \mathbf{S} \cdot \frac{\mathbf{P}}{|\mathbf{P}|}. \tag{2.10}$$

Since spin has a discrete value with regard to an axis, helicity is discrete as well. For spin-half particles like fermions, if the helicity is positive, $+\frac{\hbar}{2}$, it is called right-handed, otherwise the particle is left-handed. In other words, when the direction of momentum and spin of a particle are the same, it refers to right-handed, and vice versa. Mathematically, chirality is the sign of the projection of the spin vector onto the momentum vector, left is negative and right is positive. For massless spin-half particles, helicity is equivalent to the operator of chirality multiplied by $\frac{1}{2}$. For massless particles for which helicity is frame independent, helicity and chirality are identical, on the contrary for massive particles helicity is frame dependent and is not identical with chirality, so there is no frame dependence of the weak interactions. Rotating the left-handed and right-handed components independently makes no difference on the theory, we say that the theory has chiral symmetry

$$\begin{cases} \psi_L \longrightarrow e^{i\theta_L}\psi_L \\ \psi_R \longrightarrow \psi_R \end{cases}, \tag{2.11}$$

or

$$\begin{cases} \psi_L \longrightarrow \psi_L \\ \psi_R \longrightarrow e^{i\theta_R}\psi_R \end{cases}. \tag{2.12}$$

It can be seen that a mass term in the Lagrangian, $m\bar{\psi}\psi$ breaks chiral symmetry, therefore theories of massive fermions do not have chiral symmetry.

It appears that nature has a preference for left-handed fermions and they interact via the weak interaction. In most circumstances, two fermions of left-handed chirality interact more strongly than right-handed or opposite-handed fermions, and it implies a violation of the symmetry of the other forces of nature. Chirality does not respect the parity symmetry either. By applying the projection operator, $P^\pm = \frac{1\pm\gamma^5}{2}$, on the Dirac field, a fermion would be reduced to its left or right-handed component:

$$\begin{aligned} \psi^L(x) &= \frac{1}{2}(1-\gamma^5)\psi(x), \\ \psi^R(x) &= \frac{1}{2}(1+\gamma^5)\psi(x). \end{aligned} \tag{2.13}$$

Coupling of weak interactions to fermions is proportional to such a projection operator. The projection operator is responsible for parity symmetry violation. We must take into account that, since γ^5 is hermitian ($\gamma^5 = \gamma^{5\dagger}$) it anticommutes with γ^μ

$$\{\gamma^5, \gamma^\mu\} = 0 \longrightarrow \gamma^5\gamma^\mu = -\gamma^\mu\gamma^5. \tag{2.14}$$

Similarly for $\bar{\psi}(x) = \bar{\psi}^L(x) + \bar{\psi}^R(x)$ we can consider

$$\begin{aligned} \bar{\psi}^L(x) &= \bar{\psi}(x)\frac{(1+\gamma^5)}{2}, \\ \bar{\psi}^R(x) &= \bar{\psi}(x)\frac{(1-\gamma^5)}{2}. \end{aligned} \tag{2.15}$$

2.4 Spontaneous Symmetry Breaking

In quantum field theory, it may be possible for a field to take a nonzero global value. This global field might have a directional character, so it violates a symmetry of the Lagrangian. In such a case, we say that the field theory has a hidden or spontaneously broken symmetry. In other words, the situation in which the ground state configuration does not display the symmetry of the Hamiltonian is described by saying that the symmetry is spontaneously broken. The appearance of massless particles when a symmetry is spontaneously broken is a general result, known as the Goldstone theorem. It states that for every spontaneously broken continuous symmetry, the theory must contain a massless particle. These massless fields are called Goldstone bosons.

For a complex scalar field,

$$\phi(x) = \frac{1}{\sqrt{2}}[\phi_1(x) + i\phi_2(x)] \tag{2.16}$$

described by the Lagrangian

$$\mathcal{L} \equiv T - V(x) = (\partial_\mu\phi^*(x))(\partial^\mu\phi(x)) - \mu^2|\phi(x)|^2 - \lambda|\phi(x)|^4 \tag{2.17}$$

for which λ and μ^2 are real, this is invariant under global phase transformation. Considering the potential, stability requires that λ must be positive, but μ^2 can have either sign.

For $\mu^2 > 0$, $\phi(x) = 0$ is a stable point, but in the case that $\mu^2 < 0$, in the Lagrangian the relative sign of the $|\phi(x)|^2$ as a mass term and the kinetic energy is positive and the potential takes minima on the circle in the $(\phi_1 - \phi_2)$ plane of radius $\frac{v}{\sqrt{2}}$, such that $v^2 = -\mu^2/2\lambda$ and $\phi = 0$ does not correspond to the energy minimum. In this case the ground state is not unique. A purely real value for the ground state could be

$$\phi_0 = \left(-\frac{\mu^2}{2\lambda}\right)^{1/2} = \frac{v}{\sqrt{2}}. \tag{2.18}$$

The interpretation is that the ground state does not possess the symmetry of the Lagrangian. Choosing new coordinates we rewrite the initial field in terms of two real fields, i.e.,

$$\phi(x) = \frac{1}{\sqrt{2}}[v + \sigma(x) + i\eta(x)] \tag{2.19}$$

where the term

$$\frac{1}{\sqrt{2}}[\sigma(x)+i\eta(x)]$$

represents the quantum fluctuation about the minimum. Putting (2.19) back into (2.17) and expanding $\mathcal{L}$ about the vacuum in terms of the fields, we have

$$\mathcal{L}' = \mathcal{L}_0 + \mathcal{L}_I \tag{2.20}$$

where

$$\mathcal{L}_0 = \frac{1}{2}(\partial_\mu \sigma(x))^2 + \frac{1}{2}(\partial_\mu \eta(x))^2 - \frac{1}{2}[2\lambda v^2]\sigma^2(x) \tag{2.21}$$

and $\mathcal{L}_I$ involves some constant, cubic and quartic interaction terms in $\sigma(x)$ and $\eta(x)$ in the form of

$$\mathcal{L}_I = -\lambda v\sigma(x)[\sigma^2(x)+\eta^2(x)] - \frac{1}{4}\lambda[\sigma^2(x)+\eta^2(x)]^2. \tag{2.22}$$

It represents the interaction of the real fields with themselves.

In principle, (2.17) and (2.20) are equivalent and a transformation of the type (2.19) can not change the physics, but the $\mathcal{L}'$ unlike the $\mathcal{L}$ gives the correct picture of physics in perturbation theory and one can calculate the fluctuation around the energy minimum.

The two first terms in $\mathcal{L}_0$ feature the kinetic energy of the fields and the third one has the form of a mass term for the $\sigma(x)$ field but there is no mass term associated with the $\eta(x)$ field, because mass arises from terms that are quadratic in the field. That is, the theory involves a massless scalar as well. This is known as a Goldstone boson and is due to being along the potential well, tangential direction, that is no restriction on it. This Lagrangian was only a simple example of a theory and involving several fields, one could get several Goldstone bosons.

If we consider the Lagrangian (2.17) for three interacting real fields $\phi_i(x)$ with $i = 1,2,3$, in the case that $\mu^2 < 0$ and $\lambda > 0$, the new Lagrangian would describe a massive field of mass $(2\lambda v^2)^{1/2}$ and two massless Goldstone bosons [6].

2.5 The Higgs Mechanism

In the preceding discussion, we have seen that one of the ways the symmetry of a quantum field theory can be realized is a global symmetry, that is spontaneously broken, i.e., the vacuum state does not respect the symmetry and the particles do not form obvious symmetry multiplets. In such a theory for each generator of the spontaneously broken symmetry we have one massless scalar particle. Now we are going to consider local gauge symmetry in the theory. This leads to new possibilities. We will see that spontaneous symmetry breaking causes a massless spin 1 gauge vector boson to acquire mass. The procedure of generating massive particles is known as "Higgs mechanism".

In particle physics, the application of spontaneously broken local symmetry is in the weak interactions and this model unifies the weak interactions with electromagnetism in a single gauge theory.

Here it is considered that all of space is filled with the Higgs field. Part of the field mixes with the force carrying gauge fields to produce massive gauge bosons and the rest describes Higgs bosons.

These massive scalar bosons do not form a complete representation of the symmetry. This is the only way that vector particles like the W or Z can have mass. This mechanism is an essential part of the SM.

When the symmetry of the Higgs field is spontaneously broken the gauge boson particles, such as W and Z particles get a mass as well as quarks and leptons. It can be interpreted as a result of the interaction of the particles with the Higgs field.

As we saw for the Goldstone theorem, one of the fields was automatically massless. The spontaneous breaking of the local symmetry is accompanied by the appearance of one or more massless, spin zero scalar particles[4], Goldstone bosons, so our hope for finding mass of the weak interaction gauge field, with the Goldstone mechanism, is shattered.

Taking a closer look, we can have an amazing twist in the story. It arises when applying the idea of spontaneous symmetry breaking to the case of local gauge invariance. The studied Lagrangian in the hidden sector can be rewritten if we consider, this time, the combination of two real fields, $\phi_1(x)$ and $\phi_2(x)$, into a single complex field

$$\phi(x) = \phi_1(x) + i\phi_2(x), \tag{2.23}$$

thus

$$|\phi(x)|^2 = \phi^*(x)\phi(x) = \phi_1^2(x) + \phi_2^2(x). \tag{2.24}$$

With this new notation the Lagrangian reads

$$\mathcal{L} = (\partial_\mu \phi)^*(\partial^\mu \phi) - \mu^2[\phi^*(x)\phi(x)] - \lambda^2[\phi^*(x)\phi(x)]^2. \tag{2.25}$$

Now the rotation symmetry, that was spontaneously broken, becomes an invariance under a $U(1)$ global phase transformation

$$\phi(x) \longrightarrow e^{i\theta}\phi(x) \tag{2.26}$$

where θ is any real number. For making the equation of motion invariant under local gauge transformations

$$\phi(x) \longrightarrow e^{i\theta(x)}\phi(x) \tag{2.27}$$

by introducing a massless gauge field $A_\mu(x)$ and replacing ordinary derivatives by covariant derivatives

$$\partial_\mu \longrightarrow D_\mu = \partial_\mu + iqA_\mu(x), \tag{2.28}$$

the Lagrangian becomes

$$\mathcal{L} = (D_\mu \phi)^*(D^\mu \phi) - \mu^2[\phi^*(x)\phi(x)] - \lambda^2[\phi^*(x)\phi(x)]^2 - \frac{1}{4}F^{\mu\nu}(x)F_{\mu\nu}(x) \tag{2.29}$$

where

$$F_{\mu\nu}(x) = \partial_\nu A_\mu(x) - \partial_\mu A_\nu(x) \tag{2.30}$$

is the gauge invariant field strength tensor. This Lagrangian defines the Higgs model and is invariant under a $U(1)$ gauge transformation. Like the previous case we are interested in studying the case that $\lambda > 0$ and $\mu^2 < 0$. Now we apply the same procedure

[4]The appearance of the zero mass bosons is a consequence of the degeneracy of the vacuum.

as in section 2.4 to the locally invariant Lagrangian (2.29). We again obtain a circle of minima in the $\phi_1(x)$ and $\phi_2(x)$ space that occur for

$$\phi(x) = \phi_0 = \left(-\frac{\mu^2}{2\lambda}\right)^{1/2} e^{i\theta}, \qquad 0 \leq \theta \leq 2\pi \tag{2.31}$$

where θ describes a direction in the $(\phi_1 - \phi_2)$ plane. To apply the Feynman calculus, we have to expand the Lagrangian about a particular vacuum state. We take $\theta = 0$ and find

$$\begin{aligned} \phi_{1\min} &= \left(-\frac{\mu^2}{2\lambda}\right)^{1/2} = \frac{v}{\sqrt{2}}, \\ \phi_{2\min} &= 0. \end{aligned} \tag{2.32}$$

This choice is arbitrary and one can designate another value for θ. Defining new real fields, $\sigma(x)$ and $\eta(x)$ as before

$$\begin{aligned} \sigma(x) &= \phi_1(x) - \frac{v}{\sqrt{2}} \\ \eta(x) &= \phi_2(x) \end{aligned} \tag{2.33}$$

as fluctuations about this vacuum state, $\phi(x)$ becomes

$$\phi(x) = \frac{1}{\sqrt{2}}[v + \sigma(x) + i\eta(x)] \tag{2.34}$$

Putting it back into the Lagrangian (2.29), we would have

$$\begin{aligned} \mathcal{L} =& \frac{1}{2}[(\partial^\mu \sigma(x))(\partial_\mu \sigma(x)) - \lambda v^2 \sigma^2(x)] + \frac{1}{2}(\partial_\mu \eta(x))(\partial^\mu \eta(x)) \\ & - \frac{1}{4} F_{\mu\nu}(x) F^{\mu\nu}(x) + \frac{1}{2}(qv)^2 A_\mu(x) A^\mu(x) + qv A^\mu(x) \partial_\mu \eta(x) \\ & + \text{interaction terms} + \text{constant} \end{aligned} \tag{2.35}$$

The final constant is irrelevant and the interaction terms, which are cubic and quartic in the fields, specify various couplings of $\sigma(x)$, $\eta(x)$ and $A^\mu(x)$. The first line is the same as before and describes a scalar particle, $\sigma(x)$, of mass $(2\lambda v^2)^{1/2}$ and a massless Goldstone boson, $\eta(x)$. The second line describes the free gauge field $A_\mu(x)$, but it has acquired a mass.

Now, a question arises. Where does the mass of $A^\mu(x)$ come from? In the original Lagrangian, (2.29), we had a term of the form

$$\phi^*(x)\phi(x)A_\mu(x)A^\mu(x) \tag{2.36}$$

which would be present in the absence of spontaneous symmetry breaking (this coupling is depicted in left panel of figure 2.1), but when we consider fluctuation of the ground state, the term presented by (2.36) takes the form of the Proca mass term. There is also the quantity in $\mathcal{L}$

$$qvA^\mu(x)\partial_\mu \eta(x) \tag{2.37}$$

If we consider it as an interaction, it leads to a vertex of the form of figure 2.1 (right panel), in which the $\eta(x)$ turns into an $A(x)$. Such a bilinear in two different fields implies that we have incorrectly identified the fundamental fields, or particles, in the theory. Such an expression should be interpreted as an off-diagonal term in the mass matrix. The physical fields are those for which the mass matrix is diagonal. In other words, neither $A(x)$ nor $\eta(x)$ represents independent free particles. This difficulty is also seen in comparing the number of degrees of freedom in the two physically identical Lagrangians (2.29) and (2.35).

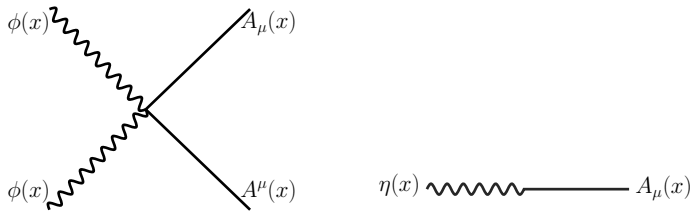

Figure 2.1: Coupling of four fields (left panel) and coupling of two independent fields (right panel).

The problem can be resolved by using the local gauge invariance of (2.29) and then eliminating $\eta(x)$ in (2.35). Rewriting equation (2.27) in terms of its real and imaginary parts

$$\begin{aligned}\phi(x) \longrightarrow \phi'(x) &= e^{i\theta(x)}\phi(x)\\ &= (\cos\theta(x) + i\sin\theta(x))(\phi_1(x) + i\phi_2(x))\\ &= [\phi_1(x)\cos\theta(x) - \phi_2(x)\sin\theta(x)] + i[\phi_1(x)\sin\theta(x) + \phi_2(x)\cos\theta(x)]\\ &= \phi_1'(x) + i\phi_2'(x) \end{aligned} \tag{2.38}$$

and picking

$$\theta = -\arctan\left(\frac{\phi_2(x)}{\phi_1(x)}\right), \tag{2.39}$$

will render $\phi'(x)$ real, which is equivalent to[5]

$$\phi_2'(x) = \eta(x) = 0. \tag{2.40}$$

In fact, a gauge transformation transforms $\phi(x)$ into a real field of the form

$$\phi(x) = \frac{1}{\sqrt{2}}[v + \sigma(x)] \tag{2.41}$$

In this particular gauge, called unitary gauge, in which the field has the form of (2.41), the Lagrangian reduces to

$$\mathcal{L} = \mathcal{L}_0(x) + \mathcal{L}_I(x) \tag{2.42}$$

[5] $\eta(x)$ is called a ghost field.

where

$$\mathcal{L}_0(x) = \frac{1}{2}[\partial^\mu \sigma(x)][\partial_\mu \sigma(x)] - \frac{1}{2}(2\lambda v^2)\sigma^2(x) - \frac{1}{4}F_{\mu\nu}(x)F^{\mu\nu}(x) + \frac{1}{2}(qv)^2 A_\mu(x)A^\mu(x). \tag{2.43}$$

It involves only the quadratic terms and can be interpreted as the free Lagrangian density of a real Klein-Gordon field $\sigma(x)$ and a real massive vector field $A_\mu(x)$. There is no such term as (2.37) in it. And the interaction part is given by

$$\mathcal{L}_I(x) = -\lambda v\sigma^3(x) - \frac{1}{4}\lambda\sigma^4(x) + \frac{1}{2}q^2 A_\mu(x)A^\mu(x)[2v\sigma(x) + \sigma^2(x)]. \tag{2.44}$$

On quantizing $\mathcal{L}_0(x)$, $\sigma(x)$ gives rise to neutral scalar bosons of mass $(2\lambda v^2)^{1/2}$ and $A_\mu(x)$ to neutral vector bosons of mass $|qv|$. In brief, by a choice of gauge, and considering gauge invariance, we have eliminated the Goldstone boson and the offending term in the Lagrangian, and the degree of freedom of $\eta(x)$ has been transferred to the massive vector field $A^\mu(x)$. Now, the number of degrees of freedom in (2.29) and (2.35) that describe definitely the same physical system are equal. A massless vector field carries two degrees of freedom, representing transverse polarizations, when $A^\mu(x)$ acquires mass, it picks up a third degree of freedom, longitudinal polarization. This extra degree of freedom comes from the Goldstone boson, which meanwhile by the Higgs mechanism disappeared from the theory. This phenomenon that a gauge field "eats" the Goldstone boson, and thereby acquires mass as well as a third polarization state, without disturbing the gauge invariance of the Lagrangian density is called the Higgs mechanism and the massive spin zero boson associated with the field $\sigma(x)$ is called a Higgs boson [7, 8].

This was an example of application of the Higgs mechanism in the spontaneous breaking of a $U(1)$ local gauge symmetry. We can repeat the same procedure to the spontaneous breaking of local $SU(2)$ symmetry. We see that we need at least one scalar $SU(2)$ doublet, a Higgs doublet field, in order to break the symmetry spontaneously[6].

2.6 The Electroweak Theory of Weinberg and Salam

In what follows we will get to know how spontaneous symmetry breaking, applying the Higgs mechanism, causes vector gauge bosons to acquire mass, but the photon remains massless. Basically the complete Lagrangian density of this model is described by

$$\mathcal{L} = \mathcal{L}^L + \mathcal{L}^B + \mathcal{L}^H + \mathcal{L}^{LH} \tag{2.45}$$

where $\mathcal{L}^L$ refers to the leptonic part of the Lagrangian density[7] and $\mathcal{L}^B$ as a Lagrangian density for gauge bosons is

$$\mathcal{L}^B = -\frac{1}{4}B_{\mu\nu}(x)B^{\mu\nu}(x) - \frac{1}{4}G_{i\mu\nu}(x)G_i^{\mu\nu}(x). \tag{2.46}$$

[6] This happens in the SM. Nowadays there exist new ideas that consider two Higgs doublets, 2HDM [1].

[7] It involves the left-handed fermion doublet and the right-handed fermion singlet.

Such a term describes gauge bosons in the absence of leptons and is invariant under $SU(2)\times U(1)$ gauge transformations. In equation (2.46), $B^{\mu\nu}(x)$ and $G_i^{\mu\nu}(x)$ are defined by

$$\begin{aligned} B^{\mu\nu}(x) &= \partial^\nu B^\mu(x) - \partial^\mu B^\nu(x) \\ G_i^{\mu\nu}(x) &= F_i^{\mu\nu}(x) + g\varepsilon_{ijk}W_j^\mu(x)W_k^\nu(x) \end{aligned} \tag{2.47}$$

with

$$F_i^{\mu\nu}(x) = \partial^\nu W_i^\mu(x) - \partial^\mu W_i^\nu(x). \tag{2.48}$$

Furthermore, $\mathcal{L}^H$ denotes the Higgs part of the Lagrangian. According to this part vector gauge bosons become massive. It can be written as

$$\mathcal{L}^H = [D^\mu\Phi(x)]^\dagger[D_\mu\Phi(x)] - \mu^2\Phi^\dagger(x)\Phi(x) - \lambda[\Phi^\dagger(x)\Phi(x)]^2 \tag{2.49}$$

where in an arbitrary gauge $\Phi(x)$ is considered a doublet of four real scalar fields $\sigma(x)$ and $\eta_i(x), i = 1,2,3$,

$$\Phi(x) = \frac{1}{\sqrt{2}}\begin{pmatrix} \eta_1(x) + i\eta_2(x) \\ \nu + \sigma(x) + i\eta_3(x) \end{pmatrix}. \tag{2.50}$$

The covariant derivative $D^\mu\Phi(x)$ is defined by

$$D^\mu\Phi(x) = [\partial^\mu + ig\tau_j W_j^\mu(x)/2 + ig'YB^\mu(x)]\Phi(x). \tag{2.51}$$

Upon quantization, these fields lead to some difficulties, i.e., the $SU(2)\times U(1)$ gauge symmetry is spontaneously broken for the vacuum state in the case $\mu^2 < 0$ and $\lambda > 0$. We can get to the point that the appropriate vacuum expectation value for the Higgs field is

$$\langle 0|\Phi(x)|0\rangle \equiv \Phi_0 = \frac{1}{\sqrt{2}}\begin{pmatrix} 0 \\ \nu \end{pmatrix} \tag{2.52}$$

where

$$\nu = \left(-\mu^2/\lambda\right)^{1/2}. \tag{2.53}$$

Since Φ_0 is neutral, the $U(1)_{\text{em}}$ symmetry with the choice $I^W = \frac{1}{2}$, $I_3^W = -\frac{1}{2}$ and $Y = \frac{1}{2}$ with generator

$$Y = \frac{Q}{e} - I_3^W \tag{2.54}$$

remains unbroken. i.e.,

$$Q\Phi_0 = 0. \tag{2.55}$$

Therefore

$$\Phi_0 \longrightarrow \Phi_0' = e^{i\alpha(x)Q}\Phi_0 = \Phi_0 \tag{2.56}$$

where $\alpha(x)$ is an arbitrary function, so that the vacuum is invariant under $U(1)_{\text{em}}$ transformations and the photon remains massless. We mention that the vacuum does not respect the $SU(2)\times U(1)$ symmetry. Here we again apply the Higgs mechanism, in analogy with section 2.5 and then in the unitary gauge we pick up the form

$$\Phi(x) = \frac{1}{\sqrt{2}}\begin{pmatrix} 0 \\ v + \sigma(x) \end{pmatrix} \tag{2.57}$$

for the isospinor scalar field about its ground state value. In the unitary gauge the $\eta_i(x)$ fields with $i = 1,2,3$ vanish. What is left is $\sigma(x)$, that gives rise to the electrically neutral, massive, spin zero Higgs scalar. Now putting (2.57) into the Lagrangian (2.45), we see that the electroweak vector bosons acquire mass, their masses are given as

$$m_W = \frac{1}{2} v g \qquad m_Z = m_W / \cos\theta_W \tag{2.58}$$

The masses predicted by the theory for m_W and m_Z are in good agreement with the experimental values. For the neutral scalar Higgs particle we have

$$m_H = (2\lambda v^2)^{1/2} \tag{2.59}$$

The neutral Higgs particle is an eigenstate of charge-parity symmetry, CP, and considered even. Great attention should be paid that the mass of the neutral Higgs boson is determined by considering only the first two terms of the potential

$$V\big(\Phi(x)\big) = \mu^2 \Phi^\dagger(x)\Phi(x) + \lambda[\Phi^\dagger(x)\Phi(x)]^2 + \ldots. \tag{2.60}$$

The value of the self-interaction constant, λ, can be determined from the Higgs mass, which now is known. Now we come to the last part of the complete Lagrangian, i.e., $\mathcal{L}^{LH}$, which is defined by

$$\begin{aligned} \mathcal{L}^{LH}(x) = &- g_l[\bar{\Psi}_l^L(x)\psi_l^R(x)\Phi(x) + \Phi^\dagger(x)\bar{\psi}_l^R(x)\Psi_l^L(x)] \\ &- g_{\nu_l}[\bar{\Psi}_l^L(x)\psi_{\nu_l}^R(x)\tilde{\Phi}(x) + \tilde{\Phi}^\dagger(x)\bar{\psi}_{\nu_l}^R(x)\Psi_l^L(x)] \end{aligned} \tag{2.61}$$

where g_l and g_{ν_l} are Yukawa coupling constants and the sum is over different types of leptons. $\Phi(x)$ and $\tilde{\Phi}(x)$ are weak isospin doublets and defined by

$$\begin{aligned} \Phi(x) &= \begin{pmatrix} \phi_a(x) \\ \phi_b(x) \end{pmatrix}, \\ \tilde{\Phi}(x) &= -i[\Phi^\dagger(x)\tau_2]^T = \begin{pmatrix} \phi_b^*(x) \\ -\phi_a^*(x) \end{pmatrix}, \end{aligned} \tag{2.62}$$

where τ_2 is the Pauli matrix and T denotes the transpose. The Lagrangian density (2.61) is invariant under $SU(2) \times U(1)$ gauge transformations. Doing some tedious calculation lead us to the point that the first line of this Lagrangian, which obviously represents coupling of two leptons to one Higgs, yields

$$-g_l \frac{v}{\sqrt{2}}[\bar{\psi}_l^L(x)\psi_l^R(x) + \bar{\psi}_l^R(x)\psi_l^L(x)] + \cdots. \tag{2.63}$$

It is equivalent to

$$-g_l \frac{v}{\sqrt{2}}\bar{\psi}_l(x)\psi_l(x). \tag{2.64}$$

The term $g_l \frac{v}{\sqrt{2}}$ refers to the lepton mass and the Yukawa coupling constant, g_l, is proportional to the lepton mass, m_l. The theory could be easily extended to involve quarks and in the same manner one can see how quarks couple to the Higgs field and acquire mass due to invariance under $SU(2) \times U(1)$ gauge transformations. That is, the Higgs coupling to the fermions is proportional to their masses.

In this theory, which is well known as the "Standard Model", the minimal choice of a single Higgs doublet is sufficient to generate masses for gauge bosons, leptons as well as quarks [7].

Chapter 3

Challenges for the Standard Model

3.1 Introduction

Why do we need to go beyond the SM?

The SM is a low-energy effective theory which happens to be renormalizable; hence highly predictive, and it describes present collider data to a remarkable accuracy. The general question to ask is whether the Higgs mechanism as depicted in the SM is a complete description of Electroweak Symmetry Breaking (EWSB) consistent with all experimental data, or there is a more fundamental underlying dynamics that mimics a Higgs-like picture at the electroweak scale. On theoretical grounds, the latter seems to be the case.

Even though no sign of new physics has been reported neither in electroweak precision nor in flavour physics, the SM is not satisfactory and it is not believed to be the ultimate theory. There is a list of unsolved problems in the physics of elementary particles [9–11] and circumventing these problems provides a vast amount of motivations for new physics Beyond the Standard Model (BSM). For certain, some of those which are most relevant to the work presented in this thesis will be emphasized below.

3.2 Baryon Asymmetry

It is evident that the idea of symmetry plays an important role in particle theory. This symmetry translates into the existence of a conservation law. To take an example, consider the electromagnetic interactions. Maxwell's equations would still be valid if we attempt to change all the positive charges into negative and vice versa. The symmetry ensures that the electric charge can not be created or destroyed and the net charge of the Universe is expected to be zero.

The laws of physics also seem to fail to distinguish between matter and anti-matter. But we know that the Universe is mostly matter-dominated and especially baryons outnumber anti-baryons. The baryon number, B, is a kind of charge which is attributed to the baryons. In the same way, if one assigns -B as the baryon number for anti-baryons, the Universe must carry a net baryon number and one would speculate that B be a conserved quantity. Thus if B is non-zero presently, it could not be zero previously; hence baryon asymmetry. In effect, annihilation between matter and antimatter has made the baryon asymmetry much greater today than in the early Universe. Baryogenesis is the

process of creating an excess of baryons over anti-baryons in the early Universe, starting from a cosmos with an equal number of both.

Sakharov conditions

In 1967 Sakharov, a Russian physicist, was the first scientist to figure out 3 necessary microscopic physical conditions for the mechanism of baryogenesis [12]. They are as follows:

- Baryon number violation: processes that change the baryon number. If all interactions conserve baryon number, there will be no baryon number excess, of course. Such processes have not yet been observed.

- C and CP violation: the laws of nature must be predisposed for an excess in matter rather than antimatter. Both C and CP must be violated. If C is conserved, creation of matter and antimatter will proceed at the same rate. Since P does not affect the total amount of matter and antimatter, there will be no baryon asymmetry either if CP is conserved.

- Departure from thermal equilibrium: the baryon-number-violating processes must be out of thermal equilibrium, non-adiabatic processes. Otherwise, in equilibrium, processes would go evenly in both particle production directions, nullifying the baryon number.

He could produce an explanation for why the early Universe had no net baryon number, and laws of physics were in fact baryon symmetric, as it expanded and cooled, an imperceptible preference for baryons emerged. Annihilation of baryons with anti-baryons, thanks to Einstein's $E = mc^2$, can be converted entirely into energy in the form of electromagnetic radiation leaving the Universe with the cosmic microwave background radiation containing billions of photons for every baryon[1]. Technically speaking, the electroweak theory entails all three clauses, but unfortunately it fails to fully explain the baryon asymmetry. Theoretical calculation as well as experimental measurement show an excess far too small to account for the observed degree of asymmetry.

The reason originates from CP violation. The origin of CP violation in the standard electroweak theory is the weak interactions between three quark families that change the charge and flavour of the quarks. CP violation in the charged current interactions occurs via the Higgs mechanism. In this picture, quarks are defined in the basis vectors of the weak interactions $U' = (U_1, U_2, U_3)$ and $D' = (D_1, D_2, D_3)$ where each quark field is a linear combination of the mass eigenstates or physical quarks, $U = (u, c, t)$ and $D = (d, s, b)$. U' and D' are constructed in such a way that U_1 is the partner of D_1, U_2 is the partner of D_2 and U_3 is the partner of D_3 in an arbitrary set of the up- and down-type quarks [8].

Rewriting the Lagrangian in terms of the physical quarks, one obtains the 3×3 CKM quark mixing matrix[2] which appears naturally from the interaction of quarks with the Higgs boson. The CKM matrix is

[1] It is the interface between particle physics and cosmology.

[2] Cabibbo-Kobayashi-Maskawa matrix.

$$V_{CKM} = \begin{pmatrix} c_{12}\,c_{13} & s_{12}\,c_{13} & s_{13}\,e^{-i\delta} \\ -s_{12}\,c_{23} - c_{12}\,s_{23}\,s_{13}\,e^{i\delta} & c_{12}\,c_{23} - s_{12}\,s_{23}\,s_{13}\,e^{i\delta} & s_{23}\,c_{13} \\ s_{12}\,s_{23} - c_{12}\,c_{23}\,s_{13}\,e^{i\delta} & -c_{12}\,s_{23} - s_{12}\,c_{23}\,s_{13}\,e^{i\delta} & c_{23}\,c_{13} \end{pmatrix} \tag{3.1}$$

where $c_{ij} = cos\theta_{ij}$, $s_{ij} = sin\theta_{ij}$ and θ_{ij} is the rotation angle in the internal space of the quark fields. The phase turns some matrix elements into complex numbers, thereby violating CP invariance. The elements of the matrix correspond to the relative coupling constants between the up-type and down-type quarks and within the SM, there is no way to determine them and they are acquired experimentally. The matrix has three independent parameters (rotation angles), and one phase which is responsible for CP violation. CP violation occurs if the quark-mixing matrix is complex and vanishes if any two quark flavours with the same charge have the same mass. Due to the small quark masses, the CP violation will be tiny in any process characterized by the weak scale and the SM will not have sufficiently large CP violation [3]. However, extensions of the SM contain new sources of CP violation [13].

3.3 Naturalness and Gauge Hierarchy Problem

Although the gauge part of the electroweak theory and the QCD sector of the SM are well established, the Higgs sector remains just a conjecture and needs to be further verified experimentally. This causes some theoretical problems such as the hierarchy problem. In particle physics, the concepts of naturalness, fine-tuning and the hierarchy problems are tightly connected.

Model building requiring specific properties and symmetries help to eliminate unphysical theories. An example of such a requirement is that the theory must be Lorentz and gauge invariant. The hierarchy problem indicates that the SM is an incomplete theory even at energies as low as the weak scale ($\sim$100 GeV). It comes from the fact that the mass of the Higgs particle obtains corrections from loop diagrams. These corrections in fact can be cancelled by fine-tuning some parameters of the model, but to most physicists this solution appears unnatural[3]. That is why there is an urge to build new theories to go beyond the SM, while reproducing all of its measured properties.

From the viewpoint of particle physics there are two fundamental energy scales in nature, the electroweak and the Planck scale, $m_{\mathrm{EW}} = 10^3$ GeV and $M_{\mathrm{Planck}} = G_{\mathrm{N}}^{-1/2} = 2.4 \times 10^{18}$ GeV, respectively. Here G_N is Newton's constant of gravity. At the Planck scale gravity becomes as strong as the gauge interactions and quantum gravitational effects can not be neglected as the SM breaks down. Different models beyond the SM have been made to describe these two scales of energies. For example, the supersymmetric theories for the weak scale are responsible for quantum theory of gravity exposed at the Planck scale. The big gap between these two scales could be populated with a number of new effective field theories, i.e., theories which are approximations of more fundamental quantum theories. In this picture, these effective theories, characterized by a cutoff scale as a regulator, could describe the dynamical symmetry breaking and therefore the pattern of masses. It is worth to bear in mind that while electroweak

[3]The hierarchy problem is sometimes referred to as naturalness or fine-tuning problem.

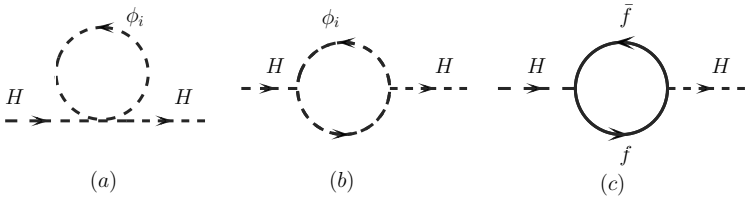

Figure 3.1: One loop radiative corrections to the Higgs squared mass parameter from a) quartic Higgs self-coupling, b) gauge boson loops, c) heavy fermion loops f.

interactions have been probed at distances $l_{\rm EW} = m_{\rm EW}^{-1}$, gravity has not yet been established at distances as small as the Planck scale ($L_{\rm Planck} = M_{\rm Planck}^{-1}$). It is well-known that the hierarchy problem has so huge a ratio of $\frac{M_{\rm Planck}}{m_{\rm EW}}$.

The hierarchy problem occurs due to sensitivity of the scalar potential to new physics. The electrically neutral part of the SM Higgs field is a complex scalar H with a potential described by (2.60)

$$V = \mu^2|\Phi|^2 + \lambda|\Phi|^4. \tag{3.2}$$

It is known that the SM requires a non-vanishing VEV for ϕ at the minimum of the potential. This will come through if $\lambda > 0$ and $\mu^2 < 0$ resulting in

$$\langle\Phi\rangle = v = \sqrt{-\mu^2/2\lambda} \tag{3.3}$$

which is approximately 246 GeV. The parameter v has the dimension of energy and sets the scale of all masses in the theory, in principle. It can be concluded that m_H^2 is of the order of $(\sim 100\ \text{GeV})^2$. The discussion so far has been at tree level (no loops).

However, the problem is that when we calculate higher order corrections, the mass squared M_H^2 of the Higgs particle receives a quadratically divergent correction in the loop expansion from virtual effect of the SM particles that couple to the Higgs field in quantum field theory. If we assume the existence of a heavy scalar particle that couples to the Higgs boson, the Feynman diagrams in figures 3.1(a) and 3.1(b) will give contributions and the Higgs boson mass squared will be sensitive to the mass of the heavy scalar particle [14].

If the Higgs field couples to a fermion, then the Feynman diagrams depicted in figure 3.1(c) introduce a correction[4]

$$\delta M_H^2 \approx -|\lambda_f|^2\, \Lambda_{UV}^2 \tag{3.4}$$

where λ_f is the Yukawa coupling proportional to g_l and g_{ν_l} (see Eq. (2.61)), and Λ_{UV} is an ultraviolet momentum cutoff whose value should not be taken to infinity, instead the finite value of the cutoff corresponds to the energy scale at which the effect of the new physics beyond the effective field theory becomes important. In other words, Λ_{UV} is the energy scale at which new physics begins to change the behaviour of the theory. All SM fermions, leptons and quarks, can enter the loop. In case of the quarks the color

[4]The numerical factor is unimportant to our argument and harmlessly is omitted.

factor is also involved, enhancing the contribution. The largest correction comes from the top quark with $\lambda_f \approx 1$.

The effect of such a contribution will be the modification of the bare mass term in the potential (2.60) by the one-loop corrected physical value

$$M^2_{\text{physical}} \approx M^2_0 - |\lambda_f|^2 \, \Lambda^2_{UV}. \tag{3.5}$$

If the cutoff is of the order of the Planck scale then this quantum correction will be orders of magnitude larger than the required value of $M^2_H \sim (100 \text{ GeV})^2$. Considering (3.5), with the assumption that v is phenomenologically fixed, implies that the Higgs coupling λ_f must be greater than unity. It follows that the Higgs sector will be strongly interacting, but it is unfavoured due to unitarity and perturbativity. The two-loop corrections involving a heavy fermion that couples indirectly with Higgs through gauge interactions could also affect the picture.

Such quadratic dependencies on the cutoff scale is present in theories with scalar fields. The quantum corrections to fermions and gauge bosons do not have direct sensitivity to the cutoff scale[5], but since these particles acquire their masses via $\langle \phi \rangle$ the entire mass spectrum of the SM is influenced by the cutoff Λ_{UV}.

Three classes of solutions seem to be plausible to circumvent the problem:

- The problem would be much less severe if the new physics takes place at a scale smaller than M_{Planck}, i.e., considering small value for the electroweak scale Λ_{UV} [15]. Then one has to invent some new physics at the cutoff scale that alters propagation in the loop. It is not easy to accomplish it in a theory that possesses the Lagrangian that solely accommodates two derivatives. Higher derivative theories usually fail either due to unitarity or causality [16].

- Introducing physics beyond the SM that contains partners to the SM particles: These new partner particles cancel off or control the quantum corrections, the quadratically divergent contributions to the Higgs scalar boson squared mass. Examples include suppersymmetry and little Higgs theories [17, 18].

- Utilizing models in which the Higgs field is removed or emerges as a composite bound state of fermions. Examples include technicolor and composite Higgs models [19].

In all these approaches, the existence of new particles are inevitable and may lead to new signals at the LHC.

3.4 The Dark Matter Problem

Since introducing a dark matter candidate is a central ingredient to this work, more details will be presented in this section.

[5] The QED is regularized by the symmetry of gauge invariance (e.g. [20]).

3.4.1 Dark Matter and Evidence for its Existence

Irrefutable evidence from cosmology reveals the existence of two fundamental states of matter in the Universe: visible or luminous, and dark matter. The former is directly observable via its interaction with electromagnetic waves, while the latter does not shine on its own, and the only way we know it exists is because of its gravitational effect and bending of light from luminous matter.

For example, galaxies in clusters move at speeds that are too high to be attributed just to the visible galaxies. Dark matter is distinguishable from empty space. The kind of materials that we experience in everyday life are made of atoms, which are in turn made of protons, neutrons, and electrons. We refer to this type of matter as baryonic. So far it looks like there are both baryonic and non-baryonic types of dark matter.

The concept of dark matter does not find any appropriate explanation in the framework of the SM. Understanding its nature and properties are fundamental to our understanding of the Universe and its fate. The nature of dark matter is elusive and we do not exactly know what it is, but during the last decade we have learned what it can not be. So a question one could ask is what dark matter is not.

- MACHOs: Some dark matter may be composed of regular matter, i.e., baryonic, but simply not give out much light. They are refereed to as MACHOs that stands for Massive Compact Halo Objects. It is some kind of astronomical bodies, essentially planets or stars, which are too dark to be seen. If there are such objects they would be detectable by creating multiple images of the distant stars or galaxies through the effect of gravitational lensing. However the search for this kind has not found enough MACHOs to explain the vast amount of dark matter that the Universe appears to contain [21, 22]. The possibility of MACHO dark matter may not be completely closed, but it now appears quite unlikely.

- CHAMPs and SIMPs: Dark matter is unlikely to be charged (CHAMP) [23] or be strongly interacting with particles [24].

- Neutrinos: The only possible dark matter candidate in electroweak theory is neutrinos. This particle could make up a fraction of the energy density of the Universe. We know that neutrinos have mass, exceedingly small compared to other particles, but non-zero nonetheless and they are oscillating from one flavour to another in flight. There are reasons that indicate neutrinos are inadequate to saturate what is needed for non-baryonic dark matter. The neutrinos possess a small rest mass[6] and are difficult to slow down by gravity, therefore traveling relativistically. Such rapidly moving entities are known as hot, and simulation of galaxy evolution in a hot dark matter universe shows galaxies forming in dense clusters with large voids between them. They also can not clump under their own gravity and thus tend to wipe out density fluctuations or structures at small scale. However this model of the Universe does not look like what the astronomers observe in practice.

[6] There is an experimental upper limit on neutrino masses $m < 2$ eV [25].

3.4.2 WIMP Dark Matter and Favoured Candidates

Other non-baryonic dark matter may be tiny, sub-atomic particles which are not a part of normal matter at all. If these tiny particles have mass and if they are numerous and cold, they could make up a large part of the dark matter widely accepted to exist. If true, then it is possible that most of the matter in the Universe is composed of some mysterious form yet to be identified. Today the main paradigm for the dark matter of the Universe has shifted to massive, non-relativistic and slowly moving particles which are very weakly interacting, WIMPs.

The intriguing possibility is that this dark matter could consist of vast quantities of subatomic particles that do not interact electromagnetically, otherwise their electromagnetic radiation would be detectable.

The evolution of galaxies would have been very different if the dark matter consists of massive, slow-moving, and therefore cold particles. A problem is that there are no such entities known in the SM. This brings us to the ideas what lie beyond the SM.

Favoured candidates

Supersymmetry: The most prosperous theory postulates the existence of supersymmetric particles, the lightest of which, LSP, includes forms that do not respond to the electromagnetic or strong forces, but they may be hundreds of times more massive than the proton. Once $SU(2) \times U(1)$ symmetry breaks, superpartners of the photon, Z, and neutral Higgs bosons, mix. Out of four such neutral states, neutralinos, the lightest one is the most popular candidate for dark matter.

Extra dimensions: Some theorists suggest that our universe may have more spatial dimensions than what we are familiar with. General relativity was extended to five-dimensional space-time in an effort to unify gravity with the force of electromagnetism [26]; later it was postulated that the fifth dimension could be hidden by being curled up [27], for example, as if each point in our familiar space were actually a tiny ring (extra dimension) which a particle could run around. Particles moving through the extra dimensions could be massive owing to their extra-dimensional momentum and its contribution to the rest mass.

In extra-dimensions theories, all the SM fields can propagate in one or more extra dimensions. These are TeV-scale scenarios featuring the Kaluza-Klein excited states of particles. These excited states of ordinary matter are known as KK modes and the lightest of them, the first KK excitation of the $U(1)_Y$ gauge boson, which is electrically neutral and non-colored, is a suitable dark matter candidate.

Exotic candidates: In addition to the mainstream candidates above, many more exotic candidates have been suggested such as WIMPzillas (with masses as large as 10^{15}GeV), Q-balls, gravitinos.

Scalar particles

Some extensions beyond the electroweak theory, while trying to explain some other shortcomings of the SM, provide a viable candidate for dark matter which, among others, meets the necessary requirements of the dark matter relic density. Like many other models for dark matter, these models are equipped with some internal symmetries

to stabilize the dark matter over the age of the Universe. Two of these models are listed here.

Little Higgs theories: The little Higgs theories, LH, are generally introduced to alleviate the Higgs hierarchy problem by putting forward a set of new particles. Contributions from new particles to the Higgs mass could eliminate the quadratic divergences at the one-loop level. With this mechanism, the LH models could stabilize the weak scale. They also give tree-level contributions to precision data. To constrain this T-parity is applied to the model. Under this transformation, the SM particles stay unaltered while all new particles become odd. In some varieties of the LH models known as "theory space", the lightest T-odd particle is stable and could contribute to the matter density of cosmos.

Inert doublet models: It is assumed that the dark matter is made of a light spinless particle known as scalar dark matter, SDM. This candidate is predicted in different extensions of the SM. They require the existence of a fundamental scalar field. These models intrinsically contain a spinless boson as a dark matter which is stable due to an imposed Z_2 symmetry.

Collisions at the large Hadron Collider at CERN may have enough energy to create them. If such a particle is found, the challenge will then be to study its properties in detail, in particular to see if it could have formed large-scale clusters of dark matter in the early Universe.

In this thesis the aim is to present two models that are trying to address some of these problems. In so doing, in the next chapter, we will study production and decay of the charged Higgs in the scope of type II 2HDM. Such a model is an extension to the SM with a new spectrum of scalar particles. This introduces new sources of CP violation and physics beyond the SM.

Next, in chapters 5 and 6, we will expand the particle content of the type II 2HDM with a new scalar doublet. Such a model will inherit many features of the 2HDM. The new scalar doublet will not obtain any vacuum expectation value and by means of an ad hoc Z_2 symmetry its lightest neutral member will be stable enough to stand as a candidate for the dark matter density of the Universe. The exploration of the viable parameter space will be briefly presented. Then in chapter 6 decay and production mechanisms of the particles will be studied. Some selected regions of the parameter space will be confronted with the latest data from direct and indirect detection experiments.

Chapter 4

Charged Higgs Production in type II 2HDM

4.1 Introduction

Albeit predictions of the SM are extremely well supported by the current data and the model has been successfully confirmed by experimental precision tests, recent theoretical and cosmological results demand its extension. Introducing only one Higgs doublet to break the symmetry in the SM is just an economical way, not the only possible one. There exists a number of motivation to extend the scalar sector of the SM [28–32]. In principle, the presence of more doublets brings up many interesting phenomenological properties. After the discovery of the Higgs boson, the exploration of an extended Higgs sector is of greater interest. In this connection, we focus our attention on the prospect of detecting the charged Higgs bosons at the LHC. We do it in the framework of the 2HDM with type II Yukawa couplings in which the Higgs sector is extended with an extra scalar doublet. In fact this chapter is an introduction to Paper I:

- Probing the charged Higgs boson at the LHC in the CP-violating type-II 2HDM [34].

In the following, we will present the fields and the potential and then we will study the possibility of detection of charged Higgs particles and identify a number of benchmark points.

4.1.1 The Fields

The Higgs sector of the SM is augmented by a new doublet with the same quantum numbers, namely weak isodoublets ($T = 1/2$) with hypercharge $Y = 1$. In fact, it builds the doublets of the 2HDM and they are expanded about their vacuum states as

$$\Phi_i = \begin{pmatrix} \varphi_i^+ \\ (v_i + \eta_i + i\chi_i)/\sqrt{2} \end{pmatrix} \quad , \quad i = 1,2. \tag{4.1}$$

Both doublets, in general, can acquire VEVs that break down the symmetry at tree level. They can be written as

$$\langle \Phi_i \rangle = \begin{pmatrix} 0 \\ v_i/\sqrt{2} \end{pmatrix} \quad , \quad i = 1,2, \tag{4.2}$$

where

$$v_1 = v\cos\beta, \qquad v_2 = v\sin\beta, \qquad v^2 = v_1^2 + v_2^2. \tag{4.3}$$

The phases of Φ_1 and Φ_2 are chosen so that v_1 and v_2 are both real and non-negative. The parameter $\tan\beta$ is the ratio of the two electroweak VEVs. We also define a mass parameter μ, by $\mu^2 = (v^2/2v_1v_2)\mathrm{Re}\, m_{12}^2$, and note that the following relation is established from the extremum condition:

$$\mathrm{Im}\, m_{12}^2 = v_1 v_2 \mathrm{Im}\, \lambda_5. \tag{4.4}$$

With the introduction of two doublets, Φ_1 and Φ_2, we are exposed to the potentially dangerous phenomenon of Flavour-Changing Neutral Current (FCNC) which experimentally is highly suppressed relative to the charged-current processes. To eliminate such an effect at tree level by Higgs mediated Yukawa couplings of the Lagrangian we impose an appropriate discrete Z_2 symmetry on the Lagrangian, potential and Yukawa interactions, in such a way that it is invariant when:

$$\begin{cases} \Phi_1 \longrightarrow -\Phi_1 \\ u_R \longrightarrow -u_R \end{cases} \tag{4.5}$$

with all other fields unchanged. The effect of the Z_2 parity is to avoid $\Phi_1 \longleftrightarrow \Phi_2$ transition [33].

4.1.2 The Potential and Parameters

The 2HDM can be classified according to its Higgs-fermion Yukawa interactions. The model we consider here is known as type-II [1] in which Φ_1 couples to down-type quarks and charged leptons ($I_3 = -1/2$) and Φ_2 couples to up-type quarks ($I_3 = 1/2$)[1]. The potential of the model reads:

$$\begin{aligned} V(\Phi_1,\Phi_2) = &-\frac{1}{2}\left\{m_{11}^2\Phi_1^\dagger\Phi_1 + m_{22}^2\Phi_2^\dagger\Phi_2 + \left[m_{12}^2\Phi_1^\dagger\Phi_2 + \text{h.c.}\right]\right\} \\ &+ \frac{\lambda_1}{2}(\Phi_1^\dagger\Phi_1)^2 + \frac{\lambda_2}{2}(\Phi_2^\dagger\Phi_2)^2 + \lambda_3(\Phi_1^\dagger\Phi_1)(\Phi_2^\dagger\Phi_2) \\ &+ \lambda_4(\Phi_1^\dagger\Phi_2)(\Phi_2^\dagger\Phi_1) + \frac{1}{2}\left[\lambda_5(\Phi_1^\dagger\Phi_2)^2 + \text{h.c.}\right]. \end{aligned} \tag{4.6}$$

In order to allow for CP-violation in the scalar sector we allow for soft Z_2 breaking by adding the mass term $m_{12}^2\Phi_1^\dagger\Phi_2 + \text{h.c.}$ to the Z_2-symmetric Lagrangian. The parameter m_{12} is generally a complex parameter and $m_{12}^2 \neq 0$.

The neutral states of Φ_1, Φ_2 will in general mix to form three neutral physical states H_1, H_2, H_3. These are linear combinations of η_1, η_2, and η_3,

$$\begin{pmatrix} H_1 \\ H_2 \\ H_3 \end{pmatrix} = R \begin{pmatrix} \eta_1 \\ \eta_2 \\ \eta_3 \end{pmatrix}, \tag{4.7}$$

where $\eta_3 \equiv -\sin\beta\chi_1 + \cos\beta\chi_2$ and the rotation matrix R is parametrized in terms of three angles α_1, α_2 and α_3 according to the convention of [72]. The model also contains a pair of charged scalar particles, $H^\pm$. Therefore, eight distinct parameters can define the parameter space of the model:

[1] Note that the 2HDM with type-II Yukawa interactions gives an effective description of the MSSM.

M_1, M_2, $M_{H^\pm}$, μ, $\tan\beta$ and α_i with $i = 1,2,3$

From this input, the value of M_3 and all λ's of the potential can be reconstructed [51]. This multi-dimensional parameter space is constrained by a number of theoretical and experimental conditions. To find the acceptable regions of the parameter space and then select a set of benchmark points, the model is faced with all the theoretical and experimental constraints in [34]. After the viable parameter space is found, we select a number of benchmark points, shown in table 4.1, in two different scenarios:

- **Low** $\tan\beta$**:** with $\tan\beta = 1, 2$.
- **High** $\tan\beta$**:** with $\tan\beta = 5, 10$.

The mass of the lightest neutral Higgs boson is taken to be $M_1 = 125$ GeV and a range of charged Higgs boson masses is validated for fixed values of $\tan\beta$, μ and M_2. When $\tan\beta$ is large ($\sim 5-10$) the model gives rise to acceptable points only if $M_{H^\pm}$, μ and M_2 are rather degenerate. Except P_9 and P_{10} that fall close to a CP-conserving limit, the other benchmark points correspond to CP-violating scenarios.

	α_1/π	α_2/π	α_3/π	$\tan\beta$	μ	M_2	$M_{H^\pm}^{\min}, M_{H^\pm}^{\max}$
P_1	0.23	0.06	0.005	1	200	300	300,325
P_2	0.35	−0.014	0.48	1	200	300	300,415
P_3	0.35	−0.015	0.496	1	200	350	300,450
P_4	0.35	−0.056	0.43	1	200	400	300,455
P_5	0.33	−0.21	0.23	1	200	450	300,470
P_6	0.27	−0.26	0.25	1	200	500	300,340
P_7	0.39	−0.07	0.33	2	200	300	300,405
P_8	0.34	−0.03	0.11	2	200	400	300,315
P_9	0.47	−0.006	0.05	10	400	400	400,440
P_{10}	0.49	−0.002	0.06	10	600	600	600,700

Table 4.1: Benchmark points selected from the allowed parameter space [34]. The mass parameter μ, the mass M_2 and allowed range of $M_{H^\pm}$ are in GeV.

4.1.3 BRs of Charged and Lightest Neutral Higgs Bosons

For the aforementioned benchmark points of the parameter space, the most relevant decay modes for which BRs $> 10^{-4}$ are determined. The branching ratios are displayed in figures 4.1 and 4.2. The results are presented for the range of $M_{H^\pm} = 300-600$ GeV. All of this range is not always inside the viable parameter space.

From figures 4.1 and 4.2, for two different values of $\tan\beta$, we can make a few observations:

- For the choice of $\tan\beta = 1$ the dominant decay mode is always tb and the branching fraction for WH_1 is about 0.1.

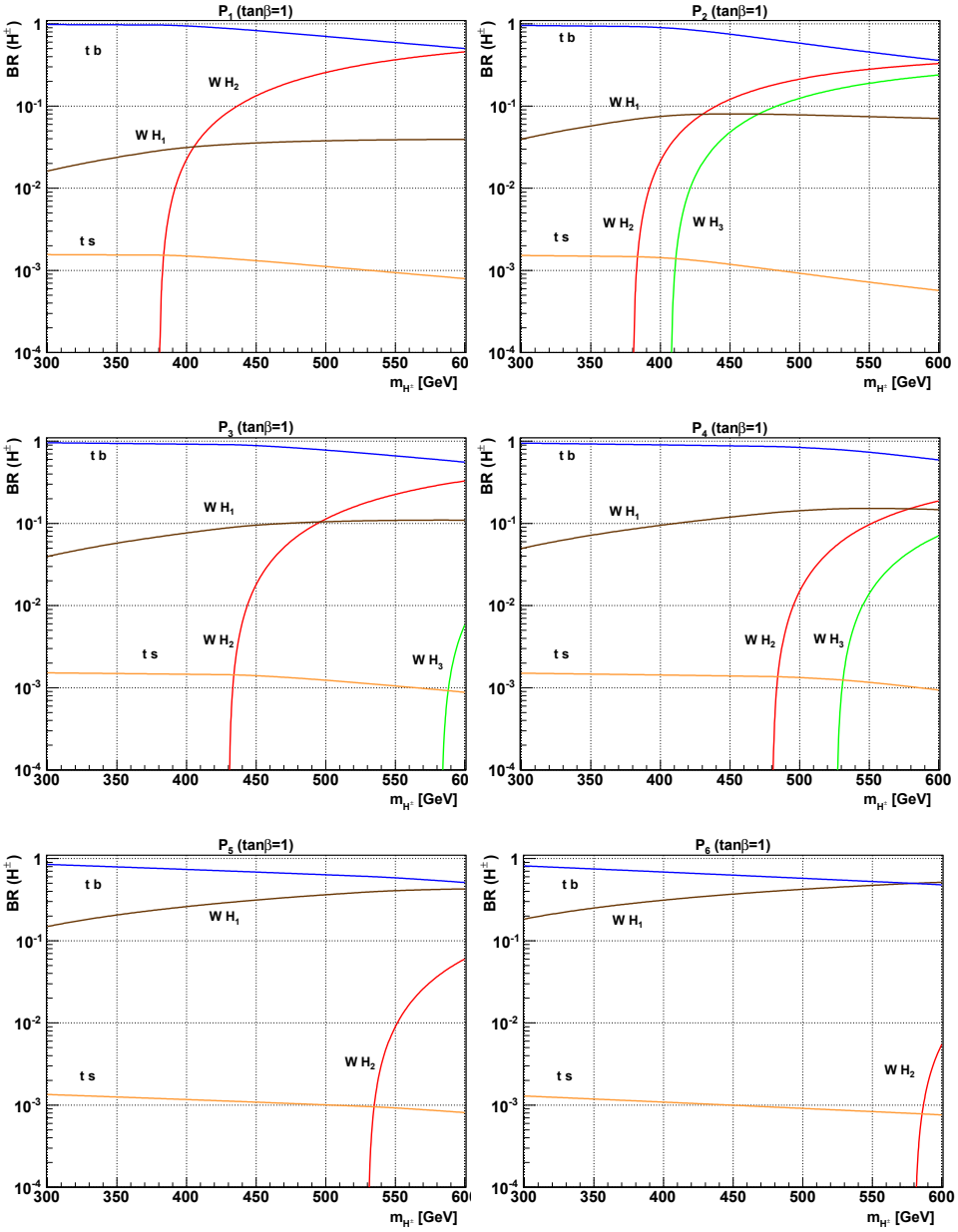

Figure 4.1: Branching ratios of the charged Higgs versus mass for six benchmark with $\tan\beta = 1$. Similar results were given in [34].

- For the choice of $\tan\beta = 2$, when $M_{H^\pm} \geq 450$ GeV, the decay channel $H^\pm \to W^\pm H_2$ becomes the dominant one, compared to $H^\pm \to tb$. It can be explained by the fact that there is a suppression of the $H^\pm \to tb$ coupling by a factor of about 2 as well as a sizeable $H^\pm \to W^\pm H_2$ coupling.
- The $\tau\nu_\tau$ decay mode strongly depends on the $\tan\beta$ value. For $\tan\beta = 2$ it reaches the 10^{-3} level.
- For the case of $\tan\beta = 2$, the branching ratio for $W^\pm H_1$ depends quite a bit on the values of other parameters.

We are interested in the phenomenology of the charged Higgs boson produced in association with vector bosons. To understand the properties of the lightest neutral Higgs boson, we collect the relevant set of H_1 branching ratios in table 4.2. We observe that the most important decay mode is always $H_1 \to b\bar{b}$. Hence we will only consider this decay channel for studying H_1 signatures.

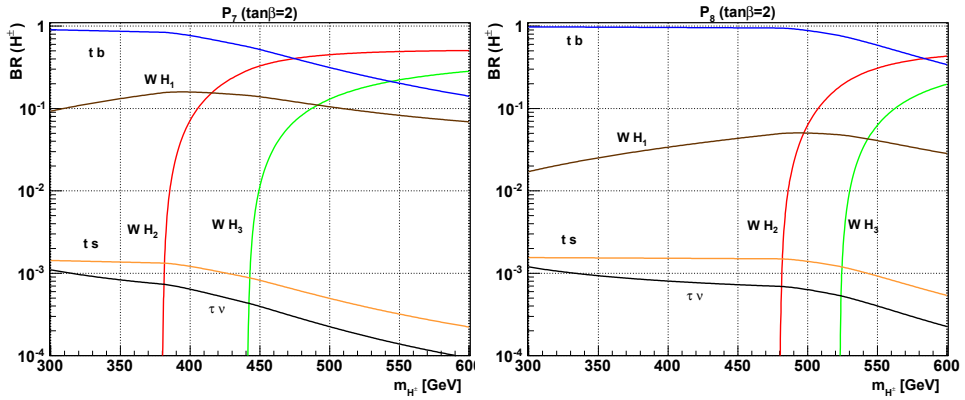

Figure 4.2: Branching ratios of the charged Higgs versus mass for two benchmark points. Here, $\tan\beta = 2$. Similar results were given in [34].

4.2 Charged Higgs Bosons at the LHC

The production and detection mechanism for the charged Higgs vary in different mass regions for the charged Higgs boson. For example, if $M_{H^\pm} < m_t - m_b$, the charged Higgs will be mainly produced by $gg \to t\bar{t}$ and $q\bar{q} \to t\bar{t}$ with subsequent decay of $t \to bH^+$ or $\bar{t} \to \bar{b}H^-$ [35]. In our study, we consider the single charged Higgs production in association with the neutral Higgs, W bosons and quarks at the LHC for the center of mass energies of $\sqrt{s} = 8$ TeV and $\sqrt{s} = 14$ TeV. The main partonic contributions to these production channels are depicted in figure 4.3. They are as follows;

$$(gg, b\bar{b}) \to H^\pm W^\mp, \tag{4.8}$$

$$q\bar{q}' \to H^\pm H_i, \tag{4.9}$$

$$gg \to H^+ b\bar{t}. \tag{4.10}$$

H_1 decay modes	P_1	P_2	P_3	P_4	P_5	P_6	P_7	P_8
$b\bar{b}$	0.5907	0.3414	0.3493	0.3528	0.4965	0.5916	0.2595	0.3697
$s\bar{s}$	0.0002	0.0001	0.0001	0.0001	0.0001	0.0002	0.0000	0.0001
$c\bar{c}$	0.0221	0.0625	0.061	0.0613	0.0451	0.0317	0.0805	0.0575
$\tau^+\tau^-$	0.0721	0.0416	0.0426	0.043	0.0605	0.0721	0.0316	0.0451
$\mu^+\mu^-$	0.0002	0.0001	0.0001	0.0001	0.0002	0.0002	0.0001	0.0002
W^+W^-	0.2145	0.3158	0.3132	0.3044	0.1809	0.1241	0.3218	0.3051
gg	0.0695	0.1944	0.1897	0.1955	0.1911	0.1621	0.2617	0.1796
ZZ	0.0262	0.0386	0.0382	0.0372	0.0221	0.0152	0.0393	0.0373
γZ	0.0017	0.0024	0.0024	0.0023	0.0014	0.0010	0.0024	0.0023
$\gamma\gamma$	0.0027	0.0032	0.0031	0.003	0.0022	0.0018	0.0030	0.0031

Table 4.2: BRs of the lightest neutral Higgs, BR$(H_1 \to XY)$, for the benchmark points. Similar results are presented in [34].

4.2.1 Cross Section Analysis for the Benchmark Points

For the above-mentioned production channels, we show the cross sections versus the charged Higgs mass in figures 4.4-4.5. The total cross section for these processes at the LHC before applying any cuts, is plotted for $\sqrt{s} = 8$ (dashed line) and for $\sqrt{s} = 14$ (solid line).

From the plots, the first lesson we obtain is that when the charged Higgs is produced in association with the neutral Higgs, as presented by Eq. (4.9) and shown in figure 4.3(b), the production cross section is low. This production channel is presented by red curves in the figures and does not seem to give rise to an observable signal; hence, it is disfavoured. The production rate is basically determined by the density of the quarks versus gluons inside protons. Since the quark density is lower than the gluon density, when the mass of the charged Higgs is increased this channel becomes suppressed. This channel is mainly mediated by the gauge bosons, W. Therefore, the offshell-ness of the intermediate W bosons reduces the rate of the production and it, in turn, results in a smaller cross section for the process (4.9). Due to the smallness of the production

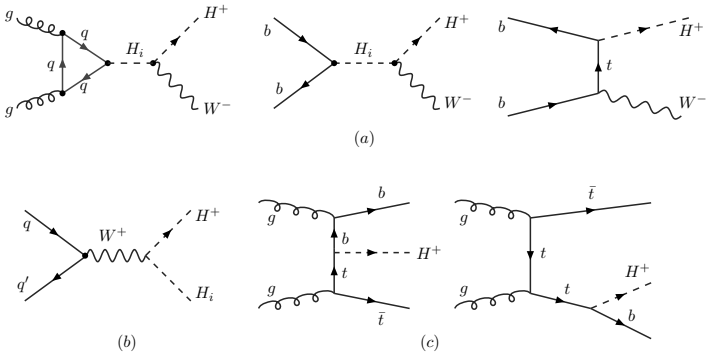

Figure 4.3: Partonic contributions to single charged Higgs production).

cross section, this channel does not have any interesting phenomenological implication at the LHC.

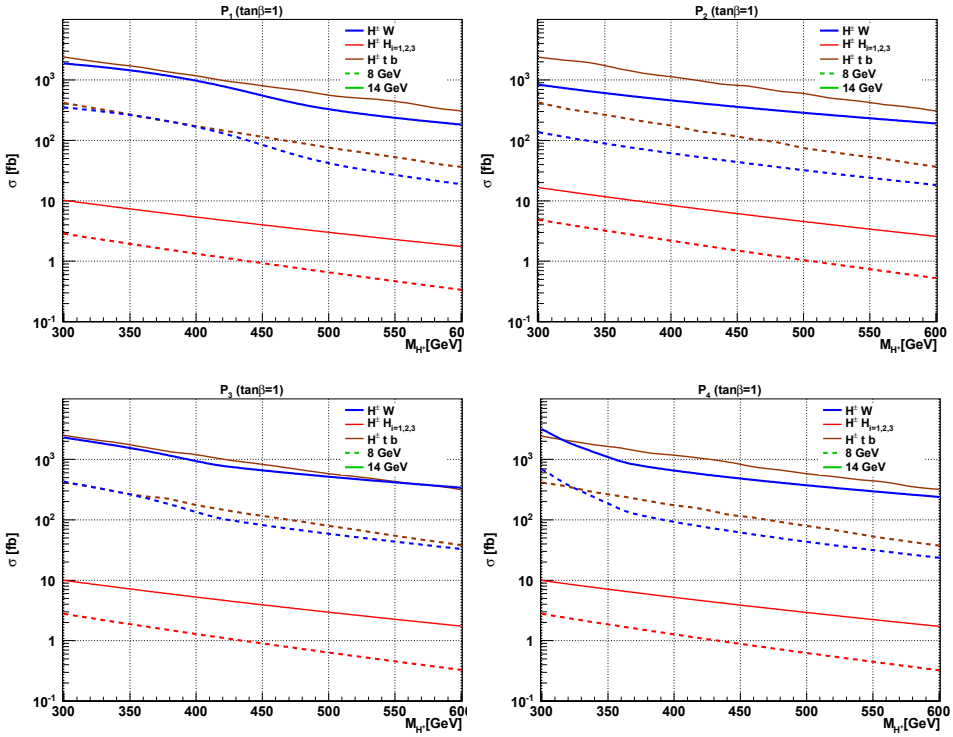

Figure 4.4: Production cross sections vs the charged Higgs mass for $\sqrt{s} = 8$ (dashed line) and $\sqrt{s} = 14$ (solid line) for benchmark points $1-4$. Similar results are presented in [34].

According to [1] the Yukawa couplings for the charged Higgs boson are expressed as

$$H^+ b\bar{t}: \qquad \frac{ig}{2\sqrt{2}m_W} V_{tb}[m_b(1+\gamma_5)\tan\beta + m_t(1-\gamma_5)\cot\beta] \tag{4.11}$$

$$H^- t\bar{b}: \qquad \frac{ig}{2\sqrt{2}m_W} V_{tb}^*[m_b(1-\gamma_5)\tan\beta + m_t(1+\gamma_5)\cot\beta] \tag{4.12}$$

and it shows that the associated production of the charged Higgs with quarks, Eq. (4.10), strongly depends on the value of $\tan\beta$. It also depends on the mass of the charged Higgs, $M_{H^\pm}$. In fact, the dominant contribution in the coupling is proportional to $m_t/\tan\beta$ and the ratio of VEVs acts as a reduction factor when $\tan\beta > 1$. The Feynman diagram for this channel is shown in figure 4.3(c). The production cross section for this channel is shown in brown in figures 4.4 and 4.5.

Let us look at associated production of a charged Higgs with a W boson, namely Eq. (4.8), the channel with a final $H^\pm W^\mp$ state. This channel is mediated by the neutral Higgs. It is shown in figure 4.3, upper left.

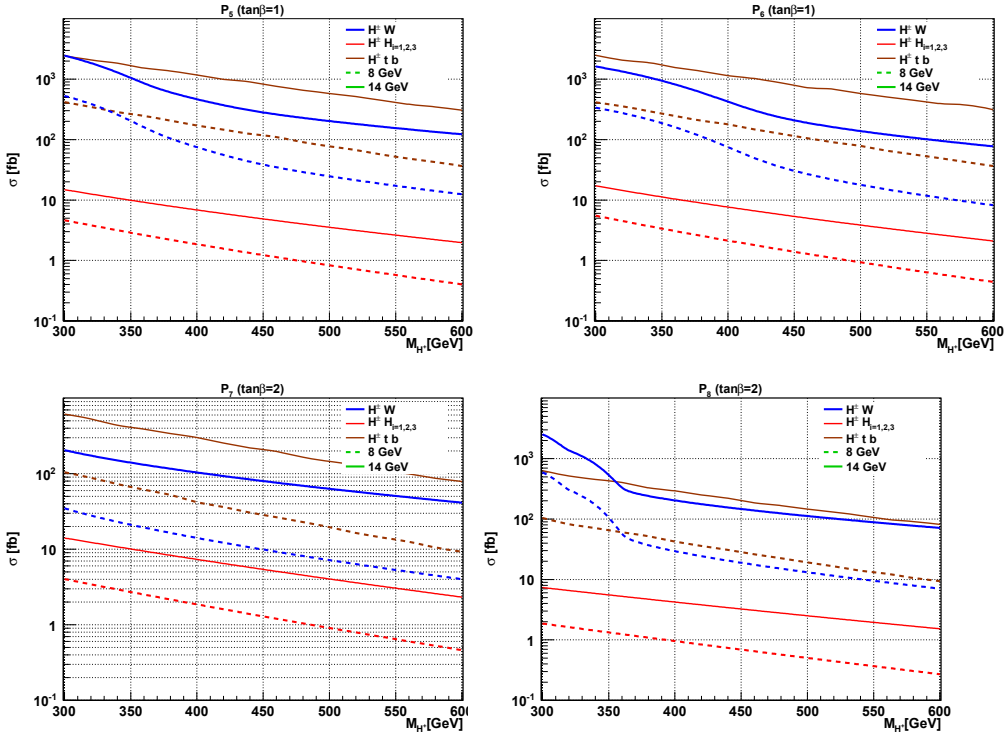

Figure 4.5: Similar to figure 4.4, for benchmark points $5-8$. Similar results are presented in [34].

The dominant production sub-processes, for the mass region selected here, are $b\bar{b} \to H^{\pm}W^{\mp}$ at tree level and $gg \to H^{\pm}W^{\mp}$ at one-loop level, depicted in 4.3(a). The latter case results in a cross section that is enhanced for the choice of high M_2 and M_3 when $m_W + M_{H^{\pm}} < M_{i=2,3}$. The cross section for this channel is shown in blue in figures 4.4 and 4.5.

In the allowed parameter space the corresponding cross sections show rather intricate behaviour. Figure 4.4 indicates that in the low-Higgs-mass scenario, when $\tan\beta = 1$ the cross section is competitive with the fermion-associated production. These qualitative conclusions also hold when $\tan\beta$ is increased to 2, despite an overall suppression due to the larger value of $\tan\beta$, involved in the $H^{+}b\bar{t}$ coupling in the form of $m_t/\tan\beta$.

The high-$\tan\beta$ benchmark points, P_9 and P_{10}, give rather low production cross sections that do not yield any useful signal after the cuts (discussed in 4.2.2) are applied.

4.2.2 Simulation of Signal and Background Events

In this section we would like to demonstrate the event analysis of the charged Higgs boson production in association with vector boson. Our preferred decay channel is $H^{\pm} \to W^{\pm}H_i$. Proton-proton collision at the LHC produces the events of interest (sig-

Generation cuts on background events
$p_b^T > 20$ GeV
$\lvert\eta_b\rvert < 2.5$
$\lvert M(b\bar{b}) - 120\rvert < 20$ GeV

Table 4.3: Generation cuts.

nal) and a large number of background events. The aim is to introduce a number of filters to examine how the signal will look like after passing through the filtering layers. We know that the charged scalar state does not belong to the particle spectrum of the SM. Hence the philosophy is that we presume the existence of new physics and try to figure out how different will the signal be from the SM signal. The SM signals are usually dubbed as background events.

Generating events:

The Monte Carlo-based (MC) data sample in our analysis, for both signal and background, was generated with the use of CalcHEP [66, 67]. It embraces all features of the process and provides a full description of the event. The generated events are in correspondence with an integrated luminosity of proton-proton collisions of 100 fb^{-1} and for both signal and background, the same Parton Distribution Function, PDF, is used, namely CTEQ6.6M [36]. The neutral Higgs boson H_1 decay branching ratio into a $b\bar{b}$ pair is about 80%, thus in the analysis we assume $H_1 \to b\bar{b}$, hence the complete process for the signal reads:

$$pp \to W^{\mp}H^{\pm} \to W^{\mp}W^{\pm}H_1 \to W^{\mp}W^{\pm}b\bar{b}. \tag{4.13}$$

For this signal, the most important background at the LHC comes from top quark pair production which gives rise to the same kind of signature;

$$pp \to t\bar{t} \to W^{\mp}W^{\pm}b\bar{b}. \tag{4.14}$$

We consider the four-jet event topology for the signal. One jet pair originates from hadronic W decay and the other W boson decays leptonically. Thus the signal event is:

$$pp \to W^{\mp}H^{\pm} \to W^{\mp}W^{\pm}H_1 \to W^{\mp}W^{\pm}b\bar{b} \to 2j + 2b + 1\ell + \text{MET}. \tag{4.15}$$

For each b or $\bar{b}$ in the final state, in the process of event analysis a b-tagging efficiency of $\sim 70\%$ is assumed. For the W bosons, the full reconstruction efficiency is adopted. For event analysis for the signal $2 \cdot 10^4$ unweighted events are generated. These events lead to a fairly nice reconstruction of the signal. For the top background, $4.5 \cdot 10^6$ unweighted events are produced. In the case of background events we have primarily considered some cuts at the level of event generation, listed in table 4.3.

In reality experiments include uncertainty and each detector has its own energy resolution. In order to estimate the effects of a real LHC-prototype detector acceptance and performance and emulate detector imperfections, we apply detector smearing to MC sample data. Therefore, the kinematic properties of of all visible final state particles are modified. The smearing is done according to a Gaussian distributions with the design energy resolution of

$$a/\sqrt{E} + b \tag{4.16}$$

where E is measured in GeV. The parameters a and b stand for stochastic and constant terms, respectively. They are determined by test-beam experiments. For a jet $(a,b) = (0.5, 0.03)$ and for leptons (electrons and muons) $(a,b) = (0.15, 0.007)$ are considered. In fact, these values are for the ATLAS detector at LHC.

The event selection criteria:

The study presented in the rest of this chapter is done differently from that of [34], i.e., firstly, not the same Monte Carlo-based data sample is used and secondly, in the results presented here we have utilized the program PYTHIA [69] and ROOT [70] in obtaining the results. That is why there are differences in what we present here with what was shown in [34]. The results are in a great agreement.

One of the most important problems in the analysis of high energy physics data is to discriminate new-physics signal against the SM background. In such an analysis, we wish to employ methods to optimize a figure of merit expressed as a function of signal and background, the signal-to-background significance ($\sim S/\sqrt{B}$), in the signal region. Significance is often used by physicists to express the cleanliness of the signal in the presence of statistical fluctuations of observed signal and background [37]. To promote the signal over background a decent set of filters is devised. We use the same selection cuts for different mass regions and both on the signal and the background events as follows:

- **Standard kinematic cuts:**

These are usually standard detector acceptance cuts. In each event, leptons are required to have

$$p_\ell^T > 15 \text{ GeV}, \qquad |\eta_\ell| < 2.5, \tag{4.17}$$

and the selected jets are required to have a jet-energy-scale-corrected

$$p_j^T > 20 \text{ GeV}, \qquad |\eta_j| < 3, \tag{4.18}$$

where p^T and η are transverse momentum and pseudo-rapidity of the particle and are defined as

$$p^T = \sqrt{p_x^2 + p_y^2}, \tag{4.19}$$

$$\eta = \frac{1}{2} \ln \left(\frac{|\mathbf{p}| + p_z}{|\mathbf{p}| + p_z} \right), \tag{4.20}$$

with the z-axis defined as the incident proton beam direction. Here $\mathbf{p}$ is the particle momentum. The condition on η is called the trigger acceptance. Cuts on p^T and η feature a detector acceptance region.

The two jets and a jet and a lepton in (4.15) are required to be separated by at least

$$|\Delta R(j,j)| > 0.5, \qquad |\Delta R(\ell,j)| > 0.5, \tag{4.21}$$

where $\Delta R = \sqrt{(\Delta\eta)^2 + (\Delta\phi)^2}$ and $\Delta\phi(\Delta\eta)$ are differences in azimuthal scattering angle (pseudo-rapidity) between jets or/and a jet and a lepton. ΔR is the parameter of separation, thus small ΔR represents particles travelling in the same direction. This cut basically has to do with detector resolution. If this criterion is not considered the two jets or a combination of a jet and a lepton will look like a single particle for the detector. This series of cuts can aid to reduce the QCD background.

- **Light Higgs reconstruction:**

In order to attempt a Higgs mass reconstruction, with the assumption that the light SM-like Higgs boson mass is 125 GeV, a filter is applied on the invariant mass of the $b\bar{b}$ pair as follows:

$$\left|M(b\bar{b}) - 125 \text{ GeV}\right| < 20 \text{ GeV}. \tag{4.22}$$

- **Hadronic W reconstruction ($W_h \to jj$):**

We demand that the final-state jets reconstruct the W boson and to do so event candidates must satisfy:

$$|M(jj) - 80 \text{ GeV}| < 20 \text{ GeV}. \tag{4.23}$$

- **The top veto**:

To reduce the backgrounds, this cut plays an important role. If $\Delta R(b_1, W_h) < \Delta R(b_2, W_h)$, it is required that

$$M(b_1 jj) > 200 \text{ GeV}, \tag{4.24}$$

and

$$M_T(b_2 \ell \nu) > 200 \text{ GeV}, \tag{4.25}$$

otherwise $1 \leftrightarrow 2$.

- **The same-hemisphere b quarks:**

Due to configuration of the signal and background, we employ another cut both on signal and background events. For a good event, we have

$$\frac{\mathbf{p}_{b_1}}{|\mathbf{p}_{b_1}|} \cdot \frac{\mathbf{p}_{b_2}}{|\mathbf{p}_{b_2}|} > 0\,. \tag{4.26}$$

In table 4.4, we show the efficiency of the previous set of cuts against the simulated background for the P_2, P_4 and P_5 points of table 4.1, for two values of charged Higgs masses, namely $M_{H^\pm} = 310$ GeV and $M_{H^\pm} = 390$ GeV[2]. Similar results are also presented in [34].

It is clearly demonstrated how the significance is influenced with imposing the cuts. There is a clear correlation between the $M_{H^\pm}$ value and the efficiency of the top veto. It is seen that the so-called “top veto" cut is the most effective cut of this set. The higher the mass, the higher the efficiency. The results of table 4.4 are in good agreement with results presented in [34]. From table 4.4, it is seen that further cuts are necessary to improve the significance. In so doing, two more signal-based cuts are considered.

[2]For completeness, the conservative limit of $M_{H^\pm} = 310$ GeV is also shown, while a recent higher order calculation of $b \to s\gamma$ puts a limit on $M_{H^\pm}$ in exclusion of values below $\sim 360 - 380$ GeV [71].

Cut	BG events	BG Eff. (%)	P_2 events	P_2 Eff. (%)	$S/\sqrt{B}$
Kinematic	366566	100	72.5, 77.2	100, 100	0.1, 0.1
H_1 reconstruction	327256	89.2	72.4, 77.1	99.9, 99.9	0.1, 0.1
W reconstruction	321294	98.1	70.9, 75.7	98.0, 98.1	0.1, 0.1
top veto	2250	0.7	20.7, 37.9	29.3, 50.1	0.4, 0.8
same-side b's	872	38.8	18.9, 35.0	90.8, 92.2	0.6, 1.1
Cut	BG events	BG Eff. (%)	P_4 events	P_4 Eff. (%)	$S/\sqrt{B}$
Kinematic	366566	100	423.1, 213.0	100, 100	0.7, 0.3
H_1 reconstruction	327256	89.2	422.9, 212.8	99.9, 99.9	0.7, 0.3
W reconstruction	321294	98.1	414.1, 209.0	97.9, 98.2	0.7, 0.3
top veto	2250	0.7	51.2, 93.9	12.3, 44.9	1.0, 1.9
same-side b's	872	38.8	46.4, 87.5	90.5, 93.1	1.5, 2.9
Cut	BG events	BG Eff. (%)	P_5 events	P_5 Eff. (%)	$S/\sqrt{B}$
Kinematic	366566	100	1247.8, 484.4	100, 100	2.0, 0.8
H_1 reconstruction	327256	89.2	1246.9, 483.8	99.9, 99.8	2.1, 0.8
W reconstruction	321294	98.1	1214.5, 475.5	97.4, 98.2	2.1, 0.8
top veto	2250	0.7	133.7, 178.2	11.0, 37.47	2.8, 3.7
same-side b's	872	38.8	124.2, 164.7	92.8, 92.4	4.2, 5.5

Table 4.4: Consecutive efficiency of the cuts imposed on the top quark background and on the benchmark points P_2, P_4 and P_5 with $M_{H^\pm} = 310$ GeV and $M_{H^\pm} = 390$ GeV. The results are consistent with [34].

- **The signal-based selections:**

The assumption is that the charged Higgs mass can be equivalently reconstructed by either the invariant mass of the four jets $(2b+2j)$ or the transverse mass of the b jets, the lepton and the MET. For the signal, either of them will always reconstruct the correct charged Higgs boson mass. It is indicated by a cross-like shape shown in figure 4.6, in which we adopt an illustrative choice of charged Higgs masses. Unlike the signal, the background events are piled up at $\sim 2m_t$. This feature motivates one to consider two more filters in eliminating the top background:

$$\mathrm{C_{squ}} = \max\left(M(b\bar{b}jj), M_T(b\bar{b}\ell\nu)\right) > M_{\mathrm{lim}} \tag{4.27}$$

and

$$\mathrm{C_{sng}} = M_T(b\bar{b}\ell\nu) > M_{\mathrm{lim}}\,. \tag{4.28}$$

We shall refer to Eq. (4.27) as squared cut and to Eq. (4.28) as single cut. The single cut of Eq. (4.28) is applied only on $M_T(b\bar{b}\ell\nu)$ because the reduction of the top background is higher compared to a similar cut on the $M(b\bar{b}jj)$ for the same numerical value of M_{lim}.

The results for signal-to-background significance, after applying the cuts $\mathrm{C_{squ}}$ and $\mathrm{C_{sng}}$, are shown in tables 4.5, 4.6 and 4.7. Several values of M_{lim} for the points P_2, P_4 and P_5 are considered and demonstrated.

What emerges is that a higher value for M_{lim} results in an increase of the significance by eliminating the top background more than the signal. It can be seen that $\mathrm{C_{squ}}$ performs always better than the single cut.

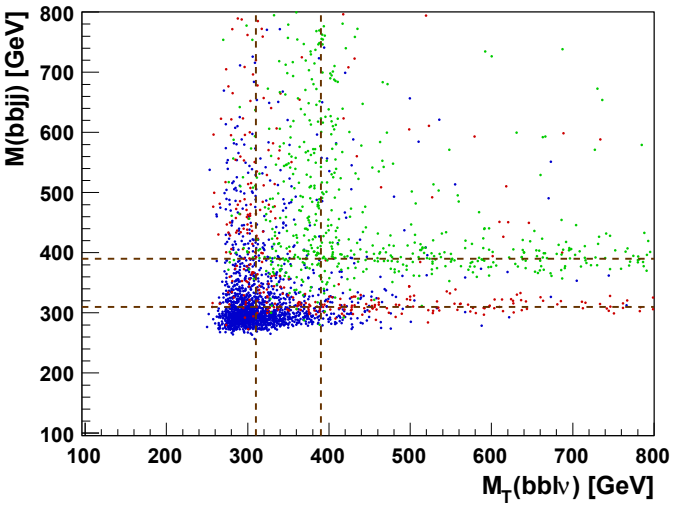

Figure 4.6: $M(b\bar{b}jj)$ vs. $M_T(b\bar{b}\ell\nu)$ after cut 5 for (unweighed) point P_5, with $M_{H^\pm} = 310$ GeV (red) and $M_{H^\pm} = 390$ GeV (green). In blue is the (unweighed) top background. Similar figure is presented in [34].

Cut		$t\bar{t}$	$P_2 = 310$ GeV		$P_2 = 390$ GeV	
		Events	Events	$S/\sqrt{B}$	Events	$S/\sqrt{B}$
$M_{\rm lim} = 450$ GeV	$C_{\rm sng}$	55.1	5.2	0.7	9.4	1.3
	$C_{\rm squ}$	114.2	8.3	0.8	15.8	1.5
$M_{\rm lim} = 500$ GeV	$C_{\rm sng}$	38.6	4.9	0.8	8.5	1.4
	$C_{\rm squ}$	82.5	7.9	0.8	14.6	1.6
$M_{\rm lim} = 550$ GeV	$C_{\rm sng}$	27.5	4.4	0.8	7.8	1.4
	$C_{\rm squ}$	59.7	7.4	0.9	13.6	1.7
$M_{\rm lim} = 600$ GeV	$C_{\rm sng}$	19.6	4.0	1.0	7.0	1.6
	$C_{\rm squ}$	42.3	6.8	1.0	12.7	1.9

Table 4.5: Comparison between $C_{\rm squ}$ and $C_{\rm sng}$ vs $M_{\rm lim}$ for P_2: surviving events and significance with respect to the background. Similar results are also presented in [34].

- **The peak cut:**

By means of a new cut the evaluation of the significance can be limited to the peak region. Such a cut is considered as:

$$|M - M_{H^\pm}| < 50 \text{ GeV}, \tag{4.29}$$

where $M = \min\left(M(b\bar{b}jj), M_T(b\bar{b}\ell\nu)\right)$ when Eq. (4.27) is employed and $M = M(b\bar{b}jj)$ when Eq. (4.28) is employed.

For all benchmark points, the result for the significance analysis is collected in table 4.8. In obtaining this table and in consistency with [34], the value $M_{\rm lim} = 600$ GeV and the selection $C_{\rm sng}$ are chosen. This choice seems to provide the best significance

Cut		$t\bar{t}$	$P_4 = 310$ GeV		$P_4 = 390$ GeV	
		Events	Events	$S/\sqrt{B}$	Events	$S/\sqrt{B}$
$M_{\rm lim} = 450$ GeV	C_{sng}	55.1	10.2	1.3	22.9	3.0
	C_{squ}	114.2	17.0	1.6	39.27	3.6
$M_{\rm lim} = 500$ GeV	C_{sng}	38.6	9.2	1.5	20.6	3.3
	C_{squ}	82.5	15.7	1.7	35.5	3.9
$M_{\rm lim} = 550$ GeV	C_{sng}	27.5	8.3	1.6	18.8	3.6
	C_{squ}	59.7	14.5	1.8	32.2	4.1
$M_{\rm lim} = 600$ GeV	C_{sng}	19.6	7.5	1.7	16.6	3.7
	C_{squ}	42.3	13.0	2.0	28.8	4.4

Table 4.6: Comparison between C_{squ} and C_{sng} vs $M_{\rm lim}$ for P_4: surviving events and significance with respect to the background. Similar results are also presented in [34].

Cut		$t\bar{t}$	$P_5 = 310$ GeV		$P_5 = 390$ GeV	
		Events	Events	$S/\sqrt{B}$	Events	$S/\sqrt{B}$
$M_{\rm lim} = 450$ GeV	C_{sng}	55.1	22.6	3.0	38.9	5.2
	C_{squ}	114.2	39.9	3.7	66.2	6.2
$M_{\rm lim} = 500$ GeV	C_{sng}	38.6	20.2	3.2	35.7	5.7
	C_{squ}	82.5	34.0	3.7	60.4	6.6
$M_{\rm lim} = 550$ GeV	C_{sng}	27.5	17.6	3.3	31.4	6.0
	C_{squ}	59.7	29.5	3.8	53.1	6.8
$M_{\rm lim} = 600$ GeV	C_{sng}	19.6	14.5	3.2	27.8	6.3
	C_{squ}	42.3	24.9	3.8	47.3	7.2

Table 4.7: Comparison between C_{squ} and C_{sng} vs $M_{\rm lim}$ for P_5: surviving events and significance with respect to the background. Similar results are also presented in [34].

while keeping a reasonable number of signal events for several of the benchmark points. The invariant mass distributions for some of the benchmark points are also plotted in figures 4.7–4.12. For each point, if possible, two values for the charged Higgs mass are considered, $M_{H^\pm} = 310$ GeV and $M_{H^\pm} = 390$ GeV.

At least three lessons emerge from the event study. They are the following:

- For P_8, with $\tan\beta = 2$ and $(M_{H_2}, M_{H^\pm}) = (400, 310)$ GeV, no considerable number of signal events is expected to survive after passing the filters.

- For P_1, P_2 ($\tan\beta = 1$, $M_{H_2} = 300$ GeV) and P_7 ($\tan\beta = 2$, $M_{H_2} = 300$ GeV) the production cross section is still large enough to give rise to observable signals with respect to the background. From the plots, it is evident that for these benchmark points the number of signal events is not above the background events.

- For P_3, P_4 and P_5, for which $\tan\beta = 1$ and we have different allowed values for M_{H_2}, when the mass of the charged Higgs is increased to higher allowed values ($M_{H^\pm} = 390$ GeV) the significance becomes larger and the signal would contain a large number of events and its peak will always lie over the background.

		$M_{H^\pm} = 310$ GeV		$M_{H^\pm} = 390$ GeV	
		Events	$S/\sqrt{B}$	Events	$S/\sqrt{B}$
$t\bar{t}$	C_{sng}	19.6			
	C_{squ}	42.3			
	C_{peak}	4.7	–	6.3	–
P_1	C_{sng}	3.7	0.8	–	–
	C_{squ}	7.2	1.1	–	–
	C_{peak}	3.5	1.6	–	–
P_2	C_{sng}	4.0	0.9	7.1	1.6
	C_{squ}	6.8	1.0	12.7	1.9
	C_{peak}	2.3	1.1	5.4	2.1
P_3	C_{sng}	8.8	2.0	18.2	4.1
	C_{squ}	15.4	2.4	30.2	4.7
	C_{peak}	5.5	2.5	13.4	5.3
P_4	C_{sng}	7.5	1.7	16.6	3.7
	C_{squ}	13.0	2.0	28.8	4.5
	C_{peak}	3.8	1.8	12.9	5.1
P_5	C_{sng}	14.5	3.2	27.8	6.2
	C_{squ}	24.9	3.9	47.3	7.2
	C_{peak}	10.23	4.7	21.1	8.4
P_6	C_{sng}	13.1	2.9	–	–
	C_{squ}	21.9	3.4	–	–
	C_{peak}	10.7	2.9	–	–
P_7	C_{sng}	2.4	0.5	5.2	1.2
	C_{squ}	4.6	0.6	10.1	1.5
	C_{peak}	2.0	0.9	4.7	1.8
P_8	C_{sng}	0	0	–	–
	C_{squ}	1.5	0.3	–	–
	C_{peak}	0	0	–	–

Table 4.8: Surviving events and their significance after the single cut of Eq. (4.28) and after the peak selection of Eq. (4.29), for all points of table 4.1, except P_9 and P_{10}. Similar results are also presented in [34].

The minor numerical differences between the results presented here and the results of [34] are due to the fact that different programs and events are used in extracting the numerical results. Apparently, the Monte Carlo precision employed in the generation of the events as well as the process of smearing the events have influenced the results.

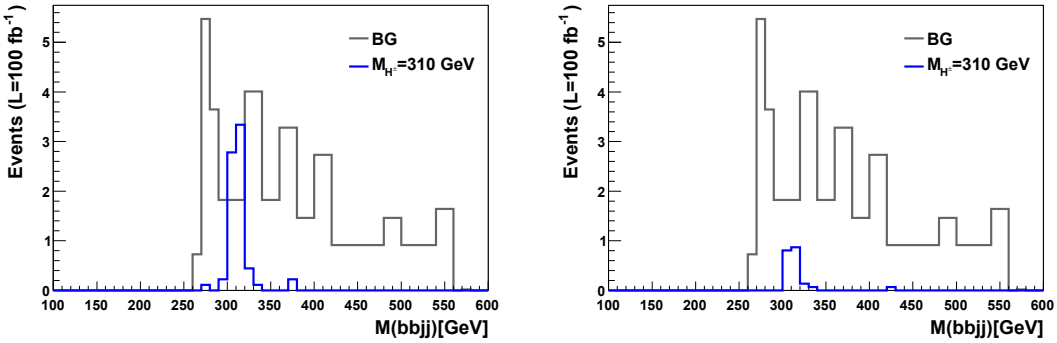

Figure 4.7: Points P_1 (left panel) and P_8 (right panel). Number of events integrated with $\mathcal{L}_{\text{int}} = 100\ \text{fb}^{-1}$ at $\sqrt{s} = 14$ TeV vs $M(b\bar{b}jj)$ for signal (colored lines) and t-quark background.

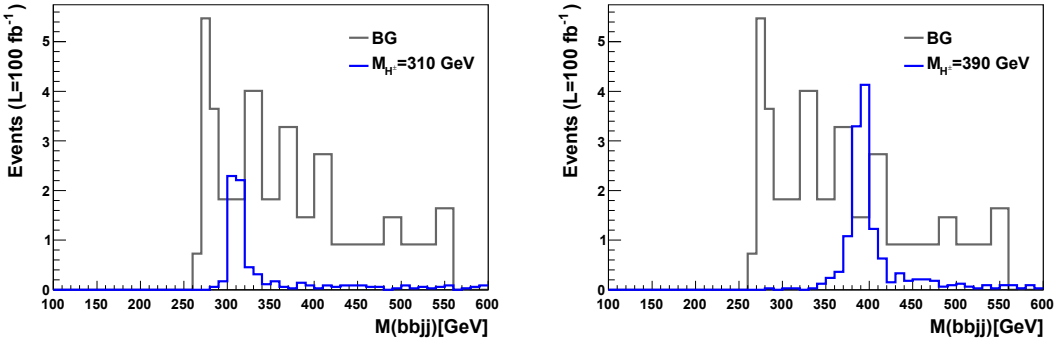

Figure 4.8: Point P_2. Similar to figure 4.7.

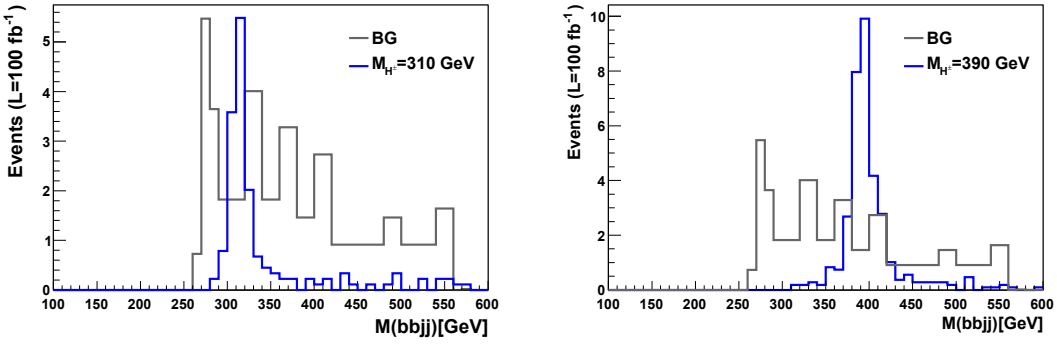

Figure 4.9: Point P_3. Similar to figure 4.7.

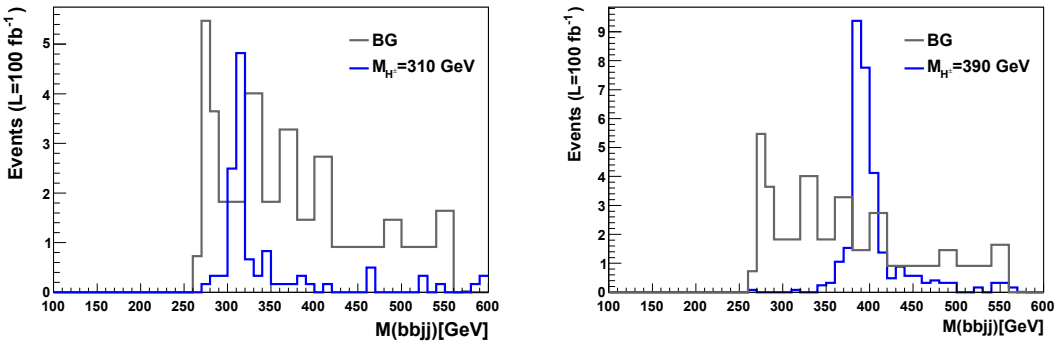

Figure 4.10: Point P_4. Similar to figure 4.7.

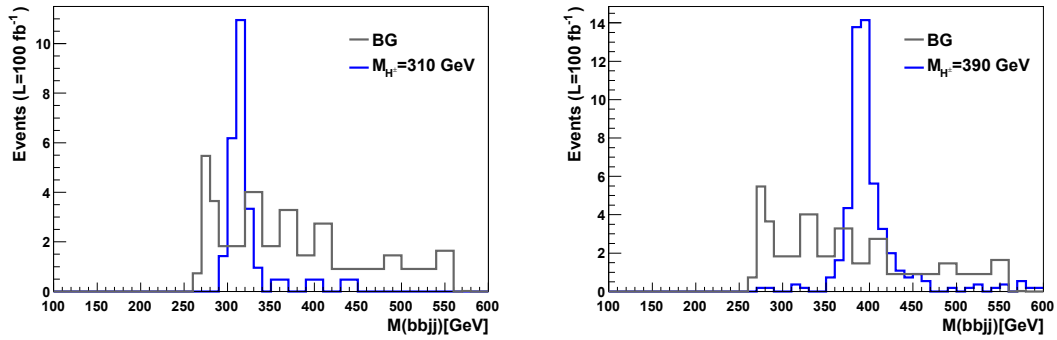

Figure 4.11: Point P_5. Similar to figure 4.7.

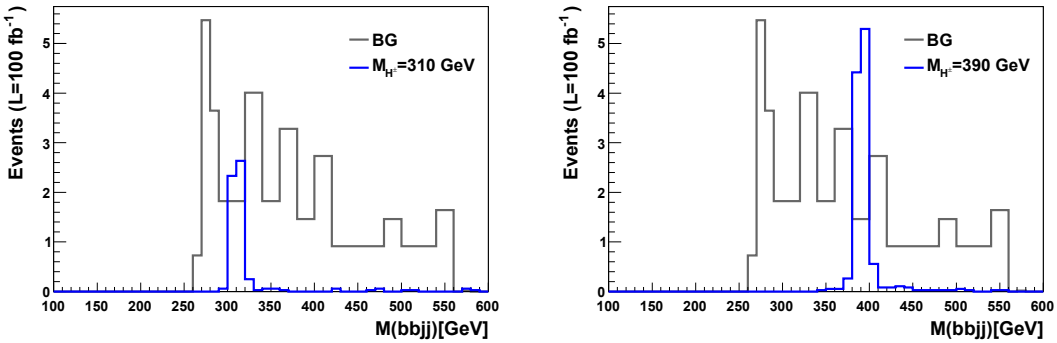

Figure 4.12: Point P_7. Similar to figure 4.7.

Chapter 5

Two Higgs Doublets plus an Inert Doublet, the IDM2

5.1 Introduction

The scalar-sector structure of the SM contains only one doublet. The choice of *one* doublet is only made for simplicity and several doublets could be included to explain the breaking of the gauge symmetry via more complicated dynamics. On the one hand, we know that the tiny CP violation present in the SM can not account for the baryon asymmetry of the Universe. On the other hand, the mysterious nature of the dark matter that comprises about 23% of the energy density of the Universe [38] is among the compelling reasons to explore what might exist beyond the SM of particle physics. It seems that the introduction of new physics that provides more sources and a wide range of CP violation to explain the baryogenesis and at the same time accommodates a dark matter candidate is a promising avenue. From this point of view, this chapter is designated to be an introduction to the second paper:

- Exploring the CP-Violating Inert-Doublet Model [39].

Here, we present a model that contains new sources of CP violation and at the same time it introduces a new scalar particle as a dark matter candidate [39]. In this chapter the goal is to present the model and to some extent discuss its viable parameter region after the discovery of the Higgs particle as well as the recent advances in dark matter detection experiments. Further experimental aspects of the model will be discussed in chapter 6 as a review of [55].

5.2 Features of the Model

The model is one of the possible ways to embed the new physics within the old paradigm to interpret the new observations. It is essentially an extension to the Inert Doublet Model (IDM) [30, 38] which has been studied extensively in [32, 41–47].

We extend this model with the introduction of a new source of CP violation in the scalar sector by means of an extra doublet. Such a model accommodates some natural features. For example, it can make the electroweak phase transition fast [40]. Basically the resulting model could also be considered as an extension of the Two-Higgs-Doublet Model (2HDM) plus an inert doublet. The resulting model will be referred to as IDM2.

5.2.1 The Fields

In the previous chapter, the Higgs sector of the type-II 2HDM was introduced. Now we extend this model with an inert doublet (dark doublet), for which the physical field appears as follows:

$$\eta = \begin{pmatrix} \eta^+ \\ (S+iA)/\sqrt{2} \end{pmatrix}. \tag{5.1}$$

The dark doublet, η, transforms under an unbroken Z_2 symmetry as

$$\eta \xrightarrow{Z_2} -\eta, \tag{5.2}$$

which ensures the doublet is inert in the sense that η couples only bilinearly to other scalars and the gauge sector. All other fields stay neutral under this transformation. The inert doublet possesses no vacuum expectation value, $\langle \eta \rangle = 0$, implying that the Z_2 symmetry associated with the inert doublet remains unbroken and therefore it does not participate in the Higgs mechanism. This feature ensures that the Z_2 parity is not spontaneously broken by a vacuum expectation value and it stabilizes the lightest neutral inert particle to contribute to the dark matter density. Basically the scalar spectrum of the model is an extension to the particle content of the 2HDM with a pair of neutral inert particles, S and A, and a pair of charged states, $\eta^\pm$ (with physical masses M_S, M_A and $M_{\eta^\pm}$)[1]. We assume that the scalar particle S is the lightest neutral one, i.e., $M_S < M_A$; hence, the dark matter candidate.

5.2.2 The Potential

The potential of the model reads;

$$V(\Phi_1, \Phi_2, \eta) = V_{12}(\Phi_1, \Phi_2) + V_3(\eta) + V_{123}(\Phi_1, \Phi_2, \eta), \tag{5.3}$$

where $V_{12}(\Phi_1, \Phi_2)$ is the 2HDM potential, described by (4.6). The inert-sector potential is

$$V_3(\eta) = m_\eta^2 \eta^\dagger \eta + \frac{\lambda_\eta}{2}(\eta^\dagger \eta)^2. \tag{5.4}$$

The mutual couplings of the inert and non-inert sectors are given by

$$\begin{aligned} V_{123}(\Phi_1, \Phi_2, \eta) = {} & \lambda_{1133}(\Phi_1^\dagger \Phi_1)(\eta^\dagger \eta) + \lambda_{2233}(\Phi_2^\dagger \Phi_2)(\eta^\dagger \eta) \\ & + \lambda_{1331}(\Phi_1^\dagger \eta)(\eta^\dagger \Phi_1) + \lambda_{2332}(\Phi_2^\dagger \eta)(\eta^\dagger \Phi_2) \\ & + \frac{1}{2}\left[\lambda_{1313}(\Phi_1^\dagger \eta)^2 + \text{h.c.}\right] + \frac{1}{2}\left[\lambda_{2323}(\Phi_2^\dagger \eta)^2 + \text{h.c.}\right]. \end{aligned} \tag{5.5}$$

The parameters λ_{1133}, λ_{2233}, λ_{1331} and λ_{2332} are real, whereas λ_{1313} and λ_{2323} can be complex. The CP is violated in the neutral non-inert scalar sector in the same way as in the 2HDM [39].

[1] IDM2 bears some similarity to the three-Higgs-doublet Weinberg model [48, 49].

5.2.3 Dark Democracy

For the quartic couplings describing the interaction between η and Φ_1 and Φ_2, we adopt a simplifying assumption, the "dark democracy" [39]:

$$\begin{aligned}\lambda_a &\equiv \lambda_{1133} = \lambda_{2233},\\ \lambda_b &\equiv \lambda_{1331} = \lambda_{2332},\\ \lambda_c &\equiv \lambda_{1313} = \lambda_{2323}.\end{aligned} \tag{5.6}$$

Following (5.5), the parameters λ_a and λ_b are real. We furthermore assume that λ_c is real. The physical masses of the dark sector are related to the parameters in the Higgs potential as

$$\begin{aligned}M_{\eta^\pm}^2 &= m_\eta^2 + \frac{1}{2}\lambda_a v^2,\\ M_S^2 &= m_\eta^2 + \frac{1}{2}(\lambda_a+\lambda_b+\lambda_c)v^2,\\ M_A^2 &= m_\eta^2 + \frac{1}{2}(\lambda_a+\lambda_b-\lambda_c)v^2,\end{aligned} \tag{5.7}$$

where m_η is a soft mass parameter of the inert sector potential (5.4), it has the dimension of mass, but it is not the mass of any particle involved in the model. The soft parameter indeed represents the bilinear couplings in the inert sector. From this point of view, it will play an important role in determining the right amount of dark matter density; hence, the viable parameter space of the model. Inverting the relations (5.7) gives rise to

$$\lambda_a = \frac{2}{v^2}\left(M_{\eta^\pm}^2 - m_\eta^2\right), \tag{5.8a}$$

$$\lambda_b = \frac{1}{v^2}\left(M_S^2 + M_A^2 - 2M_{\eta^\pm}^2\right), \tag{5.8b}$$

$$\lambda_c = \frac{1}{v^2}\left(M_S^2 - M_A^2\right). \tag{5.8c}$$

The parameters λ_a, λ_b and λ_c represent couplings between non-inert and inert sectors. These parameters are related to m_η. Thus, the couplings of the inert doublet to the non-inert Higgs sector can be expressed in terms of the mass splittings of the dark sector particles and the soft mass parameter m_η. We also define

$$\lambda_L \equiv \frac{1}{2}(\lambda_a+\lambda_b+\lambda_c) = \frac{M_S^2 - m_\eta^2}{v^2}. \tag{5.9}$$

5.3 The Parameters of the Model

The parameters of the Higgs potential are constrained by various theoretical conditions as well as the observational constraints. These conditions are requirements for a physically reasonable theory that are considered as a set of restrictions. Some of the theoretical ones are absolute (for example, positivity), whereas the experimental ones are

quantitative, and subject to experimental precision. A set of constraints are collected in Paper II [39].

The spectrum and the couplings are defined with the help of a total of 13 parameters. They are as follows:

- 2HDM sector: M_1, M_2, $M_{H^\pm}$, μ, $\tan\beta$ and α_i with $i = 1,2,3$.
- Inert sector: M_S, M_A, $M_{\eta^\pm}$, λ_η and m_η.

In order to determine allowed regions, some of these parameters are set to "interesting" values, adopted from prior studies. The rest of the parameters are scanned over in a hierarchical fashion, explained in [39]. The value of M_3 and all λ's of the 2HDM potential can be reconstructed by means of the 2HDM sector parameters [51]. The parameters λ_a, λ_b and λ_c can also be determined using the inert-sector input. We scan over the parameters and following [52, 53] focus on regions where the 2HDM is known to be consistent. In general we employ different approaches for two different dark matter mass regions [39].

5.4 Allowed Parameter Domains

In this section we review some results of [39]. At the time this study was carried out the mass of the Higgs boson was unknown and different values for M_1 were contemplated. Among different values the case of $M_1 = 120$ GeV was also studied. This was favored by electroweak SM fits [54] and is very close to the mass of the Higgs boson that is now known to be 125 GeV. That is the reason in the rest of this chapter we focus on the cases for which $M_1 = 120$ GeV. We have found only two mass regions to give rise to consistent solutions. In fact, the model is viable for medium ($M_S \sim 75$ GeV) and high mass regions ($M_S \gtrsim 550$ GeV). In the following we review these two regions.

5.4.1 Medium Dark-Matter Mass Regime

For the medium range of dark-matter mass, some selected results are shown in figure 5.1. In this figure the allowed regions are displayed in the $M_{\eta^\pm}$–m_η plane. The values of M_1 and M_S are fixed, as indicated in the figures. Since the inert scalar particle S is assumed to be the dark matter candidate it is the lightest member of the inert sector, but there is no particular hierarchy between M_A and $M_{\eta^\pm}$. In fact, in cases presented here M_A is fixed to 110 GeV adopted from [45].

An interesting feature for this mass domain is that the charged scalar from the dark sector can acquire low mass without conflicting with any constraint. It arises from the fact that the inert doublet does not develop any vacuum expectation value, hence its members have no Yukawa couplings, and are not affected by $b \to s\gamma$ constraint on the mass of charged particles contributing to this branching ratio.

In figures shown in this chapter[2], the regions in blue demonstrate the viable parameter space. In figure 5.1 the thin vertical solid lines indicate $M_{\eta^\pm} = M_S$ and the dashed line at $M_{\eta^\pm} = 70$ GeV gives the adopted experimental bound on the mass of the charged scalar [50]. The default value of M_A is also presented with a dashed line.

[2]The "holes" are presumably due to the small number of points being scanned over.

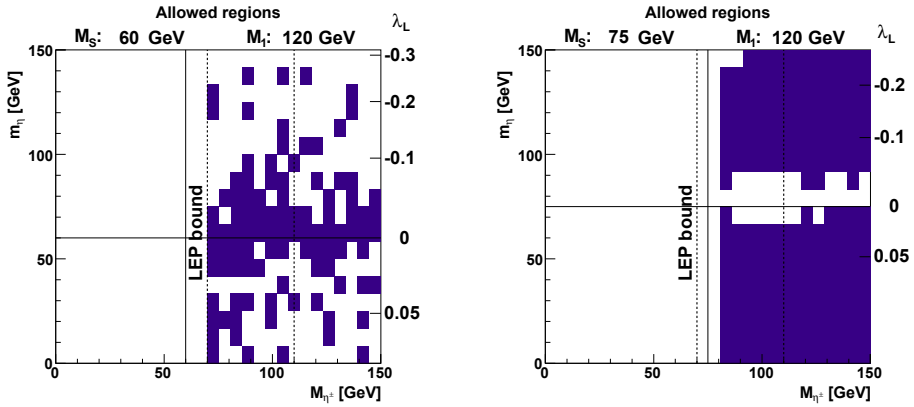

Figure 5.1: Allowed regions in the $M_{\eta^\pm} - m_\eta$ plane, for DM mass $M_S = 60$ GeV and $M_S = 75$ GeV, with lightest Higgs mass $M_1 = 120$ GeV [39].

The soft parameter m_η represents the trilinear couplings between the inert sector and the non-inert one (SSH_1). Therefore, the vertical axis in these plots is a measure of how strongly the dark matter particles annihilate via a virtual Higgs. The M_S-$M_{\eta^\pm}$ space is mainly constrained by the relic density of the dark matter and values of $M_{\eta^\pm}$ close to M_S are not acceptable. The Early-Universe annihilation, in this mass region, is controlled by SS annihilation that is most effective via the lightest neutral Higgs boson, H_1. This coupling is proportional to λ_L, which in turn is proportional to $M_S^2 - m_\eta^2$. Therefore the trilinear coupling SSH_j vanishes in the limit $m_\eta \to M_S$, but can become sizeable elsewhere.

For dark matter with mass comparable to M_W the annihilation rate to W^+W^- or ZZ can become large and the value of $\Omega_{\rm DM}$ will become inconsistent. Indeed this annihilation mechanism determines the upper cut-off of the allowed region around $M_S = 90$ GeV. It is the relic density of the dark matter that constrains the model in the low mass region and regulates the forbidden intermediate range of M_S.

The lightest neutral Higgs can be produced resonantly via SS annihilation. This is shown in the left panel of figure 5.1, in which it is illustrated that only small values of the trilinear coupling are allowed. This phenomenon disappears as M_S is further increased.

5.4.2 High Dark-Matter Mass Regime

For heavy dark matter, consistent solutions are found for $M_S \gtrsim 545$ GeV. In the high-mass region, the scanning is done in a different way from that of the low-to-medium-mass region. To avoid conflict with the dark matter and theoretical constraints, masses and the soft mass parameter m_η of the inert sector must be close to each other. This leads to having small values for λ_a, λ_b and λ_c which in turn results in an acceptable value for $\Omega_{\rm DM}$. Unlike the medium-mass region where the annihilation via a single Higgs boson is very efficient, in the heavy-mass region annihilation to two on-shell gauge bosons or two Higgs bosons play an important role in obtaining the correct amount of dark matter.

Selected results on allowed regions in the $M_{\eta^\pm}$–m_η plane are displayed in figures 5.2 and 5.3.

The other neutral and charged members of the inert doublet will also enter in the annihilation and coannihilation processes. They will be near-degenerate and several channels will be open. This will influence the way the viable parameter space is obtained in the lower and upper bounds of the heavy mass region by accommodating the observed value of $\Omega_{\rm DM}$ [39].

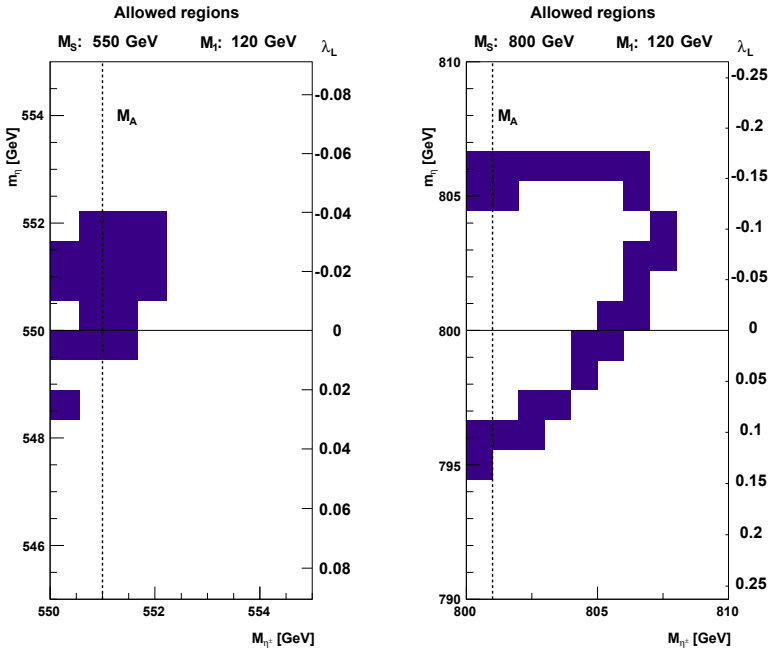

Figure 5.2: Allowed regions in the $M_{\eta^\pm} - m_\eta$ plane, for $M_S = 550$ GeV, $M_A = 551$ GeV (left panel), and $M_S = 800$ GeV, $M_A = 801$ GeV (right panel) with $M_1 = 120$ GeV. The thin solid line indicates $m_\eta = M_S$, whereas the dashed line gives $M_{\eta^\pm} = M_A$ [39].

In figure 5.3, allowed regions for dark-matter mass $M_S = 3000$ GeV, $M_A = 3001$ GeV, and $M_S = 5000$ GeV, $M_A = 5001$ GeV are shown in the $M_{\eta^\pm} - m_\eta$ plane. The solid line indicates $m_\eta = M_S$ ($\lambda_L = 0$), whereas the dashed line gives $M_{\eta^\pm} = M_A$. The unitarity requirement plays an important role in constraining the parameter space in the high mass region.

A complete set of figures and related results, concerning different mass domains of the dark matter, is presented in [39].

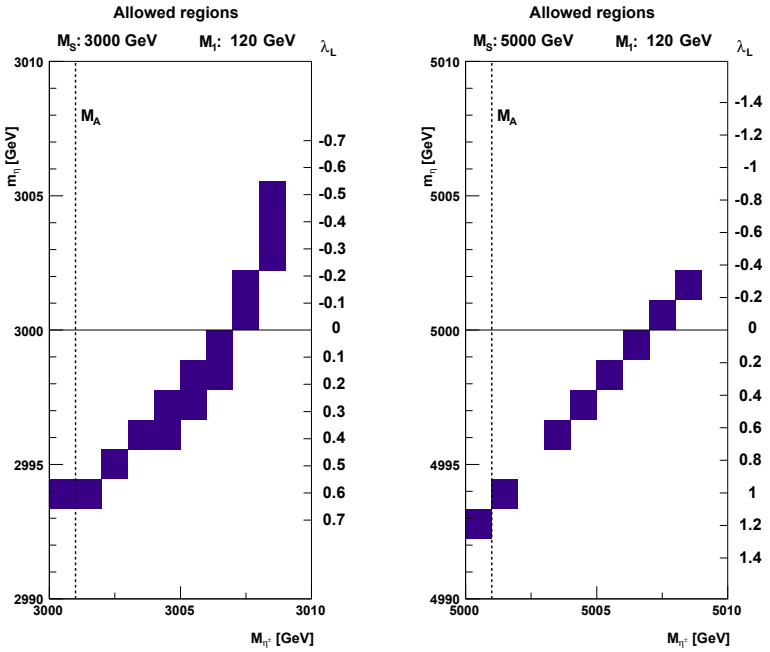

Figure 5.3: $M_S = 3000$ GeV and 5000 GeV, both with $M_1 = 120$ GeV [39].

Chapter 6

Phenomenology and LHC Prospects of the IDM2

6.1 DM Identification

During the last decades, a notable experimental effort has been dedicated to identify DM and unveil its nature. From the experimental point of view there are three possibilities to detect the DM candidate WIMP. The direct detection of the DM, the search for the DM particles scattering off the atomic nuclei, the indirect search for DM via its annihilation to SM particles and the search for DM at particle colliders. This chapter is mostly adopted from:

- Exploring the CP-Violating Inert-Doublet Model [39].
- Phenomenology of charged scalars in the CP-Violating Inert-Doublet Model [55].

Here, we shall on one hand, confront the IDM2 with bounds from direct and indirect detection experiments in the low-mass region and examine if the model is viable with respect to experimental data. On the other hand, we aim to present the signals of the IDM2 and the way inert-sector particles can be produced and traced at colliders.

6.1.1 Direct Detection

The key assumption about the direct dark-matter detection experiments is that the dark matter particles are WIMPs. In other words, they interact with ordinary matter via the weak force. The other assumption is that we have some idea of their mass and interaction cross section. The interaction cross section of WIMPs with normal baryonic matter is extremely small, but it is expected to have a non-zero value. This may enable us to detect and identify the nature of dark matter directly in a number of experiments under way. Although the sensitivity of dark matter detection has been continuously improved over the last years, until now all dedicated experiments have failed to report a positive signal[1], but detectors using different materials and detection techniques have not detected the dark matter particles. It seems there is still a long way to go, before non-detection would begin to rule out interesting WIMP candidates. Nowadays experiments are reaching the sensitivity to detect the most optimistic models for the WIMPs.

[1]Only the DAMA collaboration has reported seasonal variation in their detection rate [56–58]. DAMA does not distinguish between WIMP signal and background on an event-by-event basis. Instead, the presence of WIMPs may be inferred from the annual modulation in the rate of the lowest-energy single-scatter interactions, assuming that the backgrounds do not modulate significantly [59].

In this regard, we have chosen to confront our model with the recent CDMS-II [60] and XENON100 [61, 62] results for spin-independent scattering.

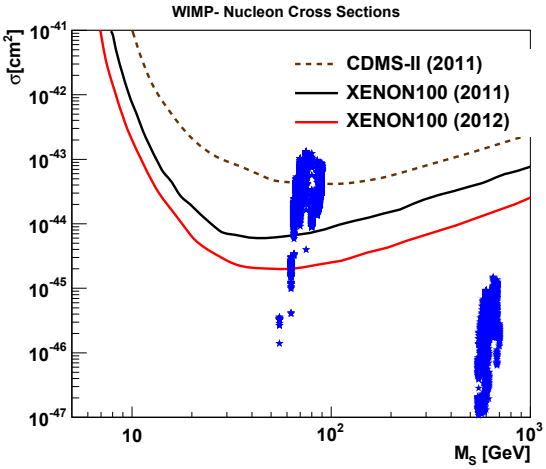

Figure 6.1: Direct-detection WIMP-nucleon cross sections compared with the CDMS-II (dashed) and XENON100 (solid) bounds.

In figure 6.1, we compare the direct-detection DM-nucleon cross sections for some of the acceptable model points with these recent constraints. These model points have passed all the theoretical and experimental constraints discussed in [55] and are different from those of [39] in the sense that the recent LHC constraints are also considered in obtaining them. For each studied value of M_S, we show a "column" of cross section values corresponding to different values of the other parameters. The mass of the lightest neutral Higgs boson is taken to be $M_1 = 125$ GeV. Values above the curves are excluded by the CDMS-II (dashed curve) or the XENON100 (solid curve) experiments. It should be noted that the black solid curve represents the 2011 XENON100 exclusion bounds [61], while the red curve represents the 2012 exclusion limits [62]. Figure 6.1 reveals that around $M_S \sim 60 - 90$ GeV, for a set of parameter points, the cross section of the dark matter particle can give a signal below the present upper limits on direct dark matter searches and much of the parameter space is compatible with the current bounds. In the high DM-mass region, the predicted cross sections are very low, implying that it would be difficult to test the model in the near future.

6.1.2 Indirect Detection

One of the indirect methods to detect dark matter is its subsequent annihilation, which could yield SM-particles like neutrinos or positrons that are potentially detectable, or decay signal in gamma-rays. In the case of photons, electrically neutral dark matter annihilates via loop processes and produces monochromatic gamma-lines, either through the annihilation into two photons ($\gamma\gamma$), a photon and a Z boson (γZ), or a photon and a Higgs boson(γH) [63].

The Fermi-LAT collaboration has determined experimental upper bounds on allowed values for various annihilation cross sections multiplied by the velocity, $\langle\sigma v\rangle$, based on various assumptions. These assumptions are referred to as "Conservative" assumptions, at 99.999% CL and 90% CL and "Stringent" exclusion [63]. In figure 6.2, we reproduce the exclusion bounds obtained for the annihilation cross section for

$$SS \to \gamma\gamma \tag{6.1}$$

according to both the conservative (upper two curves, solid lines) and the stringent approaches. We find that $\langle\sigma v\rangle_{\gamma\gamma}$ depends on λ_L^2 defined by Eq. (5.9) or in terms of the splitting

$$\langle\sigma v\rangle_{\gamma\gamma} \propto (M_S^2 - m_\eta^2)^2 \tag{6.2}$$

Here the conclusion is similar to the one for the direct-detection constraint. In figure 6.2, the model expectations are shown in blue for $M_1 = 125$ GeV and various values of M_S.

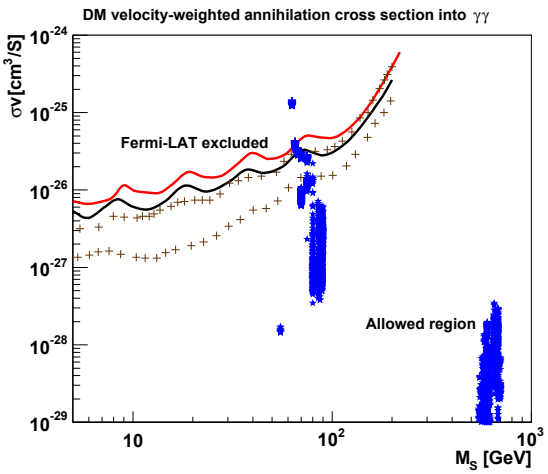

Figure 6.2: Fermi-LAT bounds on the velocity weighted annihilation cross section for $SS \to \gamma\gamma$.

6.2 Collider Signals

Due to the Z_2 symmetry imposed on the potential, members of the inert doublet (η) can only be produced in pairs at colliders

$$pp \to SSX, AAX, SAX, S\eta^\pm X, A\eta^\pm X, \eta^+\eta^- X, \tag{6.1}$$

with subsequent decay of A and $\eta^\pm$ to the lightest member, considered to be S. In particular, events with the charged scalars of the inert sector in the final state seem to be very promising for the purpose of detection. Some of these processes, for direct production, are shown in figure 6.3.

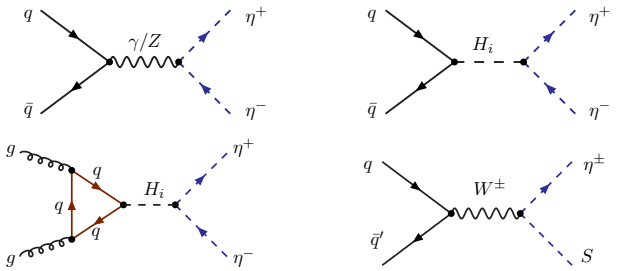

Figure 6.3: Direct production channels.

6.2.1 Charged Scalar Production at the LHC

In the following, we investigate the viability of producing charged scalar bosons at the LHC, by computing its production cross section for some representative benchmark points in the parameter space. Some of these points, given in table 6.1, are taken from [55]. They fulfill all the theoretical and experimental requirements discussed in [55].

	α_1/π	α_2/π	α_3/π	$\tan\beta$	M_2	M_3	$M_{H^\pm}$	$R_{\gamma\gamma}^{\text{2HDM}}$	$R_{\gamma\gamma}^{\text{IDM2}}$	$R_{\gamma\gamma}^{\text{IDM2}}$
P_1	0.39	−0.026	0.46	1	300	333	400	0.92	0.50	0.34
P_2	0.39	−0.009	0.025	1	300	325	400	0.91	0.50	0.34
P_3	0.37	−0.018	0.016	1	300	394	400	0.78	0.45	0.30
P_4	0.2	0.45	0.38	1	400	486	500	3.63	1.67	1.62
P_5	0.19	0.46	0.39	1	400	501	500	4.02	1.84	1.8
P_6	0.21	0.46	0.39	1	400	463	500	4.02	1.83	1.8

Table 6.1: Benchmark points selected from the allowed 2HDM parameter space. Some of these points are taken from [55]. Masses are in GeV, $\mu = 200$ GeV. Values of the ratio $R_{\gamma\gamma}$ are given for the 2HDM, as well as for IDM2. Two values of $M_{\eta^\pm}$ are considered, 100 GeV and 200 GeV.

The search for the SM Higgs boson via the diphoton decay of the Higgs boson is performed by the ATLAS and CMS collaborations [64, 65]. In Table 6.1 the value of this branching ratio, relative to that of the SM, has been presented,

$$R_{\gamma\gamma} = \frac{\Gamma(H_1 \to gg)\text{BR}(H_1 \to \gamma\gamma)}{\Gamma(H_{\text{SM}} \to gg)\text{BR}(H_{\text{SM}} \to \gamma\gamma)}. \tag{6.2}$$

The ratio, $R_{\gamma\gamma}$, is lowered by the contribution of the $\eta^\pm$ in the loop. For this study, we have taken $M_{\eta^\pm} = 100$ GeV (next-to-last column) and $M_{\eta^\pm} = 200$ GeV (last column). For comparison, its value in the absence of the $\eta^\pm$ contribution is also given.

In the following subsections, we study the production cross sections for $\eta^\pm$ in different processes. These cross sections are computed by utilizing the code CalcHEP [66, 67].

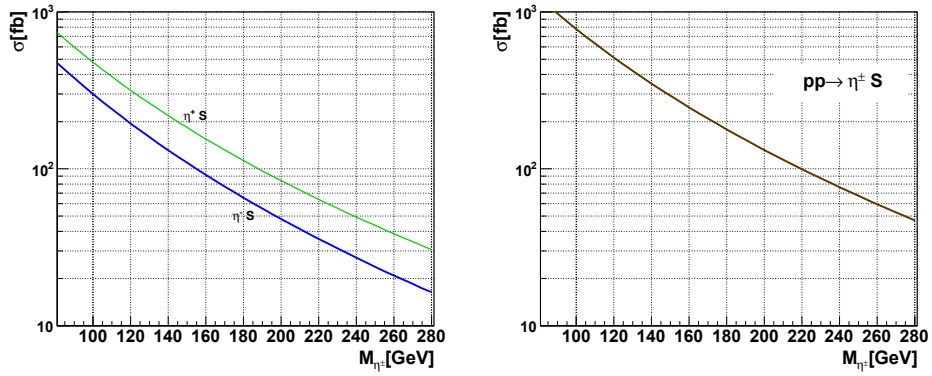

Figure 6.4: Cross sections for $\eta^+ S$ and $\eta^- S$ associated production at $\sqrt{s} = 14$ TeV. Left: Individual cross sections for $\eta^+ S$ and $\eta^- S$. Right: Sum. Similar results are shown in [55].

6.2.2 Associated production of $\eta^+ S$ and $\eta^- S$

The charged $\eta^\pm$ can be produced in association with the DM particle via an s-channel W-exchange. At the parton level we have:

$$q\bar{q}' \to W^{\pm\star} \to \eta^\pm S. \tag{6.3}$$

The typical cross sections for this process are shown in figure 6.4 for P_1 where the left panel shows the η^+ and η^- produced separately via W^+ and W^-, respectively. Since there are more u quarks than d quarks in the protons, the rate for $\eta^+ S$ production will be higher than that for $\eta^- S$ and therefore there will be more η^+ produced than η^-. The summed cross section is shown in the right panel where the cross section is of the order of $100 - 1000$ fb for $M_{\eta^\pm}$ up to a mass about 210 GeV.

6.2.3 Associated production of $\eta^+ SX$ and $\eta^- SX$:

A final state with a hard jet could be considered as well. In this case the cross section gets reduced. Typical cross sections are shown in figure 6.5 while these cuts are considered:

$$\begin{aligned} p_{\mathrm{T}}^{\mathrm{min}} &= 20 \text{ GeV}, \\ -4.5 < \eta(\text{jet}) &< 4.5. \end{aligned} \tag{6.4}$$

The reasons for the interest in these signals are at least twofold. First the observation of events of this kind should be an instant evidence of new physics and second, it could play an important role in the search for scalar dark matter, i.e., the extra jet can help in triggering this kind of interaction.

6.2.4 Pair Production of Two Charged Particles, $\eta^+ \eta^-$

The pair production mechanism at the parton level for $\eta^\pm$ can proceed as follows:

$$q\bar{q} \to \gamma^\star, Z^\star \to \eta^+ \eta^-, \tag{6.5a}$$

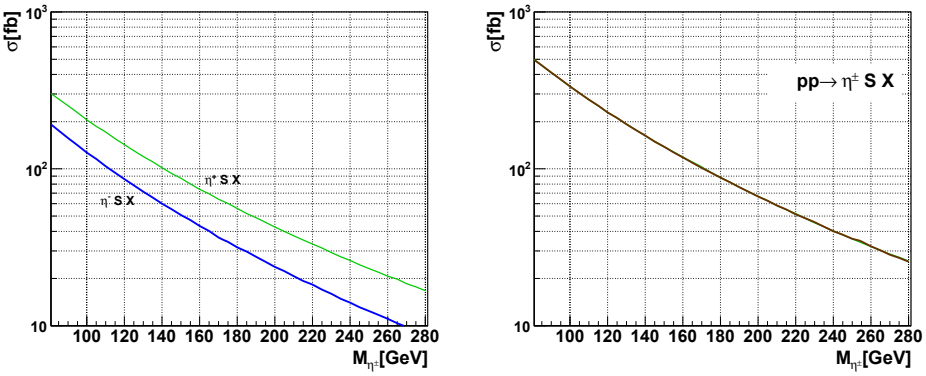

Figure 6.5: Cross sections for $\eta^+ Sj$ and $\eta^- Sj$ associated production at $\sqrt{s} = 14$ TeV. Left: Individual cross sections for $\eta^+ Sj$ and $\eta^- Sj$. Right: Sum. Similar results are shown in [55].

$$gg \to H_i^\star \to \eta^+ \eta^- \qquad i = 1,2,3. \tag{6.5b}$$

For such processes the cross section is presented in figure 6.6, for the benchmark points P_3 and P_5. The cross section depends on the soft parameter m_η, for which two values are considered, representing two different strengths of the $H_i \eta^+ \eta^-$ coupling. The shoulders are obviously due to the cut-offs from contributions involving s-channel H_2 and H_3 exchange that correspond to $2M_{\eta^\pm} = M_2$ and $2M_{\eta^\pm} = M_3$, for various values of these masses. The cross section is of the order of $100 - 500$ fb, out to a mass $M_{\eta^\pm}$ of the order of 150 GeV.

The $\eta^\pm$ can decay to $W^\pm S$. In a region of the parameter space the $W^\pm$ could be off-shell and the virtual $W^\pm$ can decay leptonically. The lepton charge is of interest in the detection of the new charged scalars and consequently the new physics.

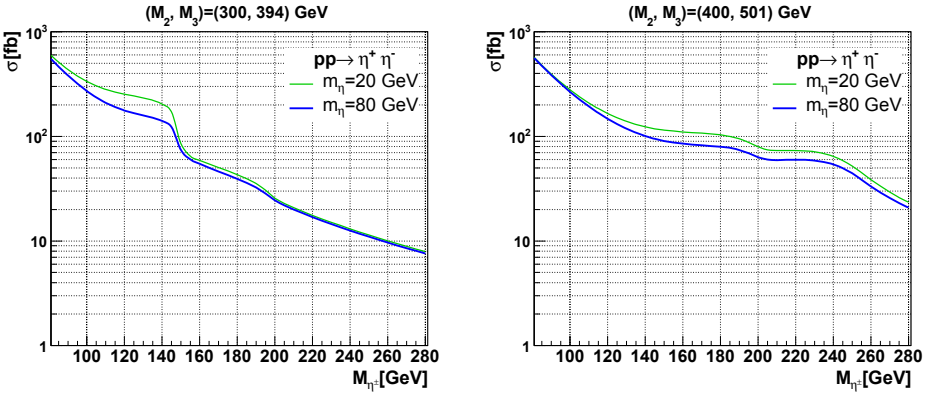

Figure 6.6: Cross sections for $\eta^+ \eta^-$ pair production at $\sqrt{s} = 14$ TeV. Left: P_3, Right: P_5. Similar results are shown in [55].

6.2.5 Decay of Charged scalars

In the region preferred by the DM, decays involving $\eta^{\pm}$ could lead to observable signals. The combination of a small mass splitting between the charged scalar, $\eta^{\pm}$, and the inert one, S, can lead to long-lived charged scalars that decay away from the interaction point and give displaced vertices in LHC detectors. In the IDM2 when the dark matter is heavy, in order to have a consistent value for Ω_{DM} a small mass splitting is preferred for inert doublet members [39]. In the case of a light dark matter it is found that in a considerable part of the parameter space the mass splitting between $\eta^{\pm}$ and S could also be small [39]. In such a favourable situation, if charged scalars are produced, they can decay to $SW^{\pm}$. The $W^{\pm}$ then decays to fermions, as depicted in figure 6.7, that may enable $\eta^{\pm}$ to be detected [55]. Depending on the mass hierar-

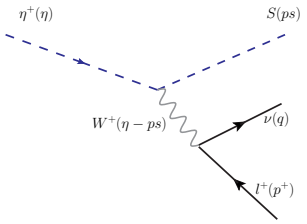

Figure 6.7: Decay of a charged scalar η^+ to the DM particle S, a charged lepton and a neutrino.

chy between particles of the inert sector, also an A could be an intermediate state [68]. Therefore the kinematically allowed decays, at the leading order, are

$$\eta^{\pm} \to Sff' \tag{6.6}$$

$$\eta^{\pm} \to Aff'. \tag{6.7}$$

Thus, the $\eta^{\pm}$ width will be:

$$\Gamma = \Gamma(\eta^{\pm} \to SW^{\pm}) + \Gamma(\eta^{\pm} \to AW^{\pm}), \tag{6.8}$$

where the W may be virtual. In figure 6.8, the branching ratios of $\eta^{\pm}$ (right panel) as well as the decay width of the $\eta^{\pm}$ (left panel) is presented. The steep rise in the width is when the W reaches threshold, at $M_{\eta^{\pm}} = M_S + M_W$. The A would in turn decay, via a virtual or real Z to the S and two fermions. Such chains would thus yield four fermions, occasionally three of which would be charged leptons. The $Sf\bar{f}'$ final state would dominate when the S is significantly lighter than the A. The oscillations in the $W^{\pm}A$ branching ratio are due to WS reaching threshold for real Ws, followed by WA reaching threshold for real Ws.

6.2.6 Displacement of the Decay Vertex

It is found that in a significant fraction of the parameter space the mass splitting between components of the inert sector could be small. In such a condition longer life time is plausible for $\eta^{\pm}$ resulting in its decay away from the interaction point. As mentioned,

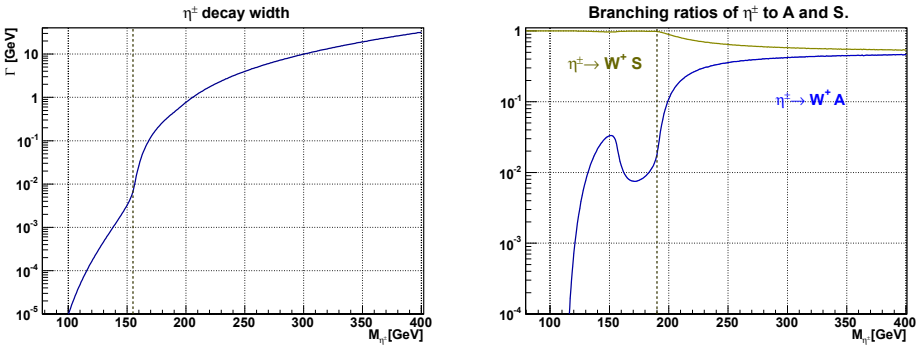

Figure 6.8: Left: Decay width of the $\eta^{\pm}$. Right: $\eta^{\pm}$ branching ratios to S or A, plus two fermions [55].

the decay involves a virtual W, and the experimental signature in this case would be the observation of an $\eta^{\pm}$ track from the production point up to its decay vertex in the detector. This will be accompanied by a kink corresponding to the decay and a track of the charged lepton, if it decays leptonically or two jets if it decays hadronically. In the case of leptonic decay such a kink does not depend on the nature of the accompanying boson being produced; either $\eta^{\mp}$, A or S, at least one kink is always there. In each case some missing energy through the presence of S's in the final state will also be present. The displacement of the decay vertex depends on the mass splitting and the velocity of $\eta^{\pm}$.

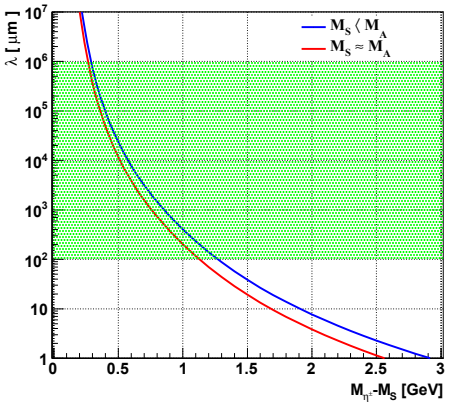

Figure 6.9: Decay length λ vs. mass splitting $M_{\eta^{\pm}}$–M_S for two relative S–A spectra [55].

The decay length, $\lambda = c\tau$, for $\eta^{\mp}$ is given in figure 6.9. If the $\eta^{\pm}$-track falls into $100\ \mu\text{m} < \lambda < 1$ m such a track, and the kink, could be seen in the detector. The shaded region corresponds to this interval, which would be the experimentally interesting range. Note that the masses should differ by not more than 1 GeV for this to be relevant. The figure 6.9 is created for the rest frame of $\eta^{\pm}$. In fact, the length of the displacement depends on the mass splitting of the inert members and the velocity of $\eta_{\pm}$.

For instance, if $M_{\eta^\pm} - M_S = 0.3$ GeV with the lifetime of $\tau = 1.23 \times 10^{-9}$ s and the velocity of $v = 0.9c$, where c is the speed of light, the decay length would be $L = 76.12$ cm. In other words, the decay length will be boosted by a factor of $\beta\gamma$ where $\beta = v/c$ and $\gamma = 1/\sqrt{1-\beta^2}$.

Chapter 7

Summary and conclusions

Our current description of the basic interactions in nature, based on the Standard Model of particle physics, is in good agreement with all known experiments. However, it is certainly fundamentally incomplete, as it does not provide enough CP violation and no candidate for the dark matter density of the Universe, among other things. After the discovery of the Higgs boson, one important question is where to go beyond the Standard Model. The answer will of course depend on what is of most interest for physics and what we are in search for!

One of the most promising ideas in theoretical particle physics is to consider more than *one* doublet to break the symmetry of the gauge theory. Such an enriched model will be capable of addressing some shortcomings of the SM. The 2HDM and IDM2 fall into such a class of theories.

In this thesis, we studied some features of these models. First, we considered the 2HDM extension of the SM and studied production cross section for the charged Higgs boson in three different channels. We saw that if the charged Higgs bosons are produced at the LHC, they will decay to SM particles. We considered a specific decay mode and performed an event study. A set of carefully devised filters could help us to distinguish the signals against the SM background. We showed the results for some selected regions of the parameter space and concluded that in most of them the signal lies above the background.

Second, the IDM2 was introduced and its viable parameter space was explored. The model was required to satisfy the observed dark matter relic density, among all other theoretical and experimental conditions. The model is valid in two different regions for the dark matter mass. The members of the inert doublet can be pair-produced at the LHC. In some region of the parameter space, when the masses of these particles are close to each other, the charged member can decay away from the interaction point.

The decay products could be leptons and missing energy or two jets and missing energy. Depending on the mass of the charged scalar and the phase space, the two jets could be treated as two separate jets or an effective mono-jet.

It might leave some signals enabling these particles to be detected.

Bibliography

[1] J. F. Gunion, H. E. Haber, G. L. Kane and S. Dawson, Front. Phys. **80**, 1 (2000). 1, 6, 4.1.2, 4.2.1

[2] A. Djouadi, Phys. Rept. **457**, 1 (2008) [arXiv:hep-ph/0503172]. 1

[3] M. B. Gavela, P. Hernandez, J. Orloff and O. Pene, Mod. Phys. Lett. A **9**, 795 (1994) [arXiv:hep-ph/9312215]. 1, 3.2

[4] H. Weyl, Sitzungsber. Preuss. Akad. Wiss. Berlin (Math. Phys.) **1918**, 465 (1918). 2.2

[5] C. -N. Yang and R. L. Mills, Phys. Rev. **96**, 191 (1954). 2.2

[6] F. Halzen and A. D. Martin, *New York, USA: Wiley (1984) 396p* 2.4

[7] F. Mandl and G. Shaw, Chichester, UK: Wiley (2010) 478 p. 2.5, 2.6

[8] M. E. Peskin and D. V. Schroeder, Reading, USA: Addison-Wesley (1995) 842 p 2.5, 3.2

[9] S. Troitsky, Phys. Usp. **55**, 72 (2012) [Usp. Fiz. Nauk **182**, 77 (2012)] [arXiv:1112.4515 [hep-ph]]. 3.1

[10] K. Nakamura *et al.* [Particle Data Group Collaboration], J. Phys. G **37**, 075021 (2010). 3.1

[11] A. Pomarol, CERN Yellow Report CERN-2012-001, 115-151 [arXiv:1202.1391 [hep-ph]]. 3.1

[12] A. D. Sakharov, Pisma Zh. Eksp. Teor. Fiz. **5**, 32 (1967) [JETP Lett. **5**, 24 (1967 SOPUA,34,392-393.1991 UFNAA,161,61-64.1991)]. 3.2

[13] Y. Grossman, Y. Nir and R. Rattazzi, Adv. Ser. Direct. High Energy Phys. **15**, 755 (1998) [arXiv:hep-ph/9701231]; Y. Nir, [arXiv:hep-ph/9911321]. 3.2

[14] A. Djouadi, Phys. Rept. **459**, 1 (2008) [hep-ph/0503173]. 3.3

[15] C. Csaki, arXiv:hep-ph/0404096. 3.3

[16] D.A. Eliezer and R.P. Woodard, Nucl. Phys. B **325**, 389 (1989). 3.3

[17] S. P. Martin, arXiv:hep-ph/9709356. 3.3

[18] M. Perelstein, Prog. Part. Nucl. Phys. **58**, 247 (2007) [arXiv:hep-ph/0512128]. 3.3

[19] For reviews, C. T. Hill and E. H. Simmons, Phys. Rept. **381**, 235 (2003) [Erratum-ibid. **390**, 553 (2004)] [arXiv:hep-ph/0203079]; K. D. Lane, arXiv:hep-ph/9401324; K. Lane, arXiv:hep-ph/0202255. 3.3

[20] I. J. R. Aitchison and A. J. G. Hey, *Bristol, UK: IOP (2003) 406 p* 5

[21] P. Tisserand *et al.* [EROS-2 Collaboration], arXiv:astro-ph/0607207. 3.4.1

[22] C. Alcock *et al.* [MACHO Collaboration], arXiv:astro-ph/9803082. 3.4.1

[23] S. Dimopoulos, D. Eichler, R. Esmailzadeh and G. D. Starkman, Phys. Rev. D **41**, 2388 (1990). 3.4.1

[24] G. D. Starkman, A. Gould, R. Esmailzadeh and S. Dimopoulos, Phys. Rev. D **41**, 3594 (1990). 3.4.1

[25] W. M. Yao *et al.* [Particle Data Group], J. Phys. G **33**, 1 (2006). 6

[26] O. Klein, Z. Phys. **37**, 895 (1926) [Surveys High Energ. Phys. **5**, 241 (1986)]. 3.4.2

[27] L. Randall and R. Sundrum, Phys. Rev. Lett. **83**, 4690 (1999) [hep-th/9906064]. 3.4.2

[28] R. S. Gupta and J. D. Wells, Phys. Rev. D **81** (2010) 055012. 4.1

[29] F. J. Botella, G. C. Branco and M. N. Rebelo, Phys. Lett. B **687** (2010) 194. 4.1

[30] R. Barbieri, L. J. Hall and V. S. Rychkov, Phys. Rev. D **74** (2006) 015007 [arXiv:hep-ph/0603188]. 4.1, 5.2

[31] E. Ma, Phys. Rev. D **73** (2006) 077301 [arXiv:hep-ph/0601225]. 4.1

[32] Q. H. Cao, E. Ma and G. Rajasekaran, Phys. Rev. D **76** (2007) 095011 [arXiv:0708.2939 [hep-ph]]. 4.1, 5.2

[33] S. L. Glashow and S. Weinberg, Phys. Rev. D **15**, 1958 (1977). 4.1.1

[34] L. Basso, A. Lipniacka, F. Mahmoudi, S. Moretti, P. Osland, G. M. Pruna and M. Purmohammadi, arXiv:1205.6569 [hep-ph]. (document), 4.1, 4.1.2, 4.1, 4.1, 4.2, 4.2, 4.4, 4.5, 4.2.2, 4.2.2, 4.4, 4.6, 4.5, 4.2.2, 4.6, 4.7, 4.8, 4.2.2

[35] Z. Kunszt and F. Zwirner, Nucl. Phys. **B385**, 3 (1992), and references cited therein. 4.2

[36] P. M. Nadolsky *et al.*, Phys. Rev. **D78**, 013004 (2008), arXiv:0802.0007. 4.2.2

[37] I. Narsky, physics/0507157. 4.2.2

[38] N. G. Deshpande and E. Ma, Phys. Rev. D **18**, 2574 (1978). 5.1, 5.2

[39] B. Grzadkowski, O. M. Ogreid and P. Osland, Phys. Rev. D **80** (2009) 055013 [arXiv:0904.2173 [hep-ph]]. (document), 5.1, 5.2.2, 5.2.3, 5.3, 5.4, 5.1, 5.4.2, 5.2, 5.4.2, 5.3, 6.1, 6.1.1, 6.2.5

[40] L. Fromme, S. J. Huber and M. Seniuch, JHEP **0611**, 038 (2006) [hep-ph/0605242]. 5.2

[41] M. Cirelli, N. Fornengo and A. Strumia, Nucl. Phys. B **753**, 178 (2006) [arXiv:hep-ph/0512090]. 5.2

[42] L. Lopez Honorez, E. Nezri, J. F. Oliver and M. H. G. Tytgat, JCAP **0702**, 028 (2007) [arXiv:hep-ph/0612275]. 5.2

[43] T. Hambye and M. H. G. Tytgat, Phys. Lett. B **659**, 651 (2008) [arXiv:0707.0633 [hep-ph]]. 5.2

[44] S. Andreas, T. Hambye and M. H. G. Tytgat, JCAP **0810**, 034 (2008) [arXiv:0808.0255 [hep-ph]]. 5.2

[45] E. Lundstrom, M. Gustafsson and J. Edsjo, Phys. Rev. D **79**, 035013 (2009) [arXiv:0810.3924 [hep-ph]]. 5.2, 5.4.1

[46] T. Hambye, F. S. Ling, L. Lopez Honorez and J. Rocher, JHEP **0907**, 090 (2009) [arXiv:0903.4010 [hep-ph]]. 5.2

[47] L. Lopez-Honorez and C. E. Yaguna, JCAP **1101**, 002 (2011). [arXiv:1011.1411 [hep-ph]]. 5.2

[48] S. Weinberg, Phys. Rev. Lett. **37**, 657 (1976). 1

[49] G. C. Branco, Phys. Rev. D **22**, 2901 (1980). 1

[50] A. Pierce and J. Thaler, JHEP **0708**, 026 (2007) [arXiv:hep-ph/0703056]. 5.4.1

[51] W. Khater and P. Osland, Nucl. Phys. B **661** (2003) 209 [arXiv:hep-ph/0302004]. 4.1.2, 5.3

[52] A. W. El Kaffas, P. Osland and O. M. Ogreid, Phys. Rev. D **76**, 095001 (2007) [arXiv:0706.2997 [hep-ph]]. 5.3

[53] A. W. El Kaffas, O. M. Ogreid and P. Osland, [arXiv:0709.4203 [hep-ph]]. 5.3

[54] C. Amsler *et al.* [Particle Data Group], Phys. Lett. B **667**, 1 (2008).

[55] P. Osland, A. Pukhov, G. M. Pruna and M. Purmohammadi, JHEP **1304** (2013) 040 [arXiv:1302.3713 [hep-ph]]. 5.4
(document), 5.1, 6.1, 6.1.1, 6.2.1, 6.1, 6.4, 6.5, 6.6, 6.2.5, 6.8, 6.9

[56] R. Bernabei *et al.* [DAMA Collaboration], INFN-AE-98-23. R. Bernabei, P. Belli, F. Cappella, R. Cerulli, F. Montecchia, F. Nozzoli, A. Incicchitti and D. Prosperi *et al.*, Int. J. Mod. Phys. D **13**, 2127 (2004) [astro-ph/0501412]. 1

[57] R. Bernabei, P. Belli, F. Montecchia, F. Nozzoli, F. Cappella, A. Incicchitti, D. Prosperi and R. Cerulli *et al.*, 1

[58] R. Bernabei, P. Belli, F. Montecchia, F. Nozzoli, F. Cappella, A. d'Angelo, A. Incicchitti and D. Prosperi *et al.*, Int. J. Mod. Phys. Conf. Ser. **12**, 37 (2012). 1

[59] R. W. Schnee, arXiv:1101.5205 [astro-ph.CO]. 1

[60] Z. Ahmed *et al.* [The CDMS-II Collaboration], Science **327**, 1619-1621 (2010). [arXiv:0912.3592 [astro-ph.CO]]. 6.1.1

[61] E. Aprile *et al.* [XENON100 Collaboration], Phys. Rev. Lett. **107**, 131302 (2011). [arXiv:1104.2549 [astro-ph.CO]]. 6.1.1, 6.1.1

[62] L. S. Lavina [for the XENON100 Collaboration], arXiv:1305.0224 [hep-ex]. 6.1.1, 6.1.1

[63] A. A. Abdo *et al.* [Fermi-LAT Collaboration], JCAP **1004**, 014 (2010) [arXiv:1002.4415 [astro-ph.CO]]. 6.1.2

[64] G. Aad *et al.* [ATLAS Collaboration], Phys. Lett. B **716**, 1 (2012) [arXiv:1207.7214 [hep-ex]]. 6.2.1

[65] S. Chatrchyan *et al.* [CMS Collaboration], Phys. Lett. B **716**, 30 (2012) [arXiv:1207.7235 [hep-ex]]. 6.2.1

[66] A. Pukhov, (2004), arXiv:hep-ph/0412191. 4.2.2, 6.2.1

[67] A. Belyaev, N. D. Christensen and A. Pukhov, Comput. Phys. Commun. **184**, 1729 (2013) [arXiv:1207.6082 [hep-ph]]. 4.2.2, 6.2.1

[68] B. Grzadkowski, O. M. Ogreid, P. Osland, A. Pukhov, M. Purmohammadi, JHEP **1106**, 003 (2011). [arXiv:1012.4680 [hep-ph]]. 6.2.5

[69] T. Sjostrand, S. Mrenna and P. Z. Skands, JHEP **0605**, 026 (2006) [hep-ph/0603175]. 4.2.2

[70] R. Brun, F. Rademakers and S. Panacek, "ROOT, an object oriented data analysis framework,"; R. Brun and F. Rademakers, Nucl. Instrum. Meth. A **389**, 81 (1997). 4.2.2

[71] T. Hermann, M. Misiak and M. Steinhauser, JHEP **1211**, 036 (2012) [arXiv:1208.2788 [hep-ph]]. 2

[72] E. Accomando *et al.*, arXiv:hep-ph/0608079. 4.1.2

Scientific results